

# GCON: Differentially Private Graph Convolutional Network via Objective Perturbation

Jianxin Wei  
National University of Singapore  
jianxinwei@comp.nus.edu.sg

Ergute Bao  
National University of Singapore  
ergute@comp.nus.edu.sg

Yizheng Zhu  
National University of Singapore  
zhuyizheng@gmail.com

Yin Yang  
Hamad Bin Khalifa University  
yyang@hbku.edu.qa

Xiaokui Xiao  
National University of Singapore  
xkxiao@nus.edu.sg

Kuntai Cai  
National University of Singapore  
caikt@comp.nus.edu.sg

Beng Chin Ooi  
National University of Singapore  
ooibc@comp.nus.edu.sg

## ABSTRACT

Graph Convolutional Networks (GCNs) are a popular machine learning model with a wide range of applications in graph analytics, including healthcare, transportation, and finance. Similar to other neural networks, a GCN may memorize parts of the training data through its model weights. Thus, when the underlying graph data contains sensitive information such as interpersonal relationships, a GCN trained without privacy-protection measures could be exploited to extract private data, leading to potential violations of privacy regulations such as GDPR.

To defend against such attacks, a promising approach is to train the GCN with differential privacy (DP), which is a rigorous framework that provides strong privacy protection by injecting random noise into the trained model weights. However, training a large graph neural network under DP is a highly challenging task. Existing solutions either introduce random perturbations in the graph topology, which leads to severe distortions of the network’s message passing, or inject randomness into each neighborhood aggregation operation, which leads to a high noise scale when the GCN performs multiple levels of aggregations.

Motivated by this, we propose GCON, a novel and effective solution for training GCNs with edge differential privacy. The main idea is to (i) convert the GCN training process into a convex optimization problem, and then (ii) apply the classic idea of perturbing the objective function to satisfy DP. Step (i) is performed by carefully choosing the graph convolution schemes from the graph analytics literature, including Simple Graph Convolution (SGC) and personalized propagation of neural predictions (PPNP), which not only establishes the convexity of the optimization problem but also effectively limits the sensitivity of the objective function. Step (ii) is significantly more challenging, and we tackle it through a sophisticated theoretical analysis that quantifies the impact of an edge modification on the graph convolution results; then, GCON samples the noise vector accordingly from a multi-dimensional hypersphere whose radius follows the Erlang distribution. Extensive experiments using multiple benchmark datasets demonstrate GCON’s consistent and superior performance over existing solutions in a wide variety of settings.

## KEYWORDS

Graph Convolutional Network; Differential Privacy

## 1 INTRODUCTION

Graph analytics has promising applications in various domains such as medicine [41], social networks [3], finance [44], and transportation [18]. In particular, a graph  $G = (V, E)$  comprises a vertex set  $V$  (often representing entities such as user profiles) and an edge set  $E$  (e.g., connections between users). Each vertex in  $V$  is also commonly associated with features or labels (e.g., attributes and types of users). In many applications, connections between individual vertices can be sensitive information. For instance, on a social network, a user may not want to disclose her/his connection with a particular person, political party, or activist group. In such scenarios, the graph analytics results must not leak the individuals’ private connections. This paper focuses on the training and release of graph convolutional networks (GCNs) [26], which is a popular deep learning solution that achieves state-of-the-art performance for common graph analytic tasks such as vertex classification [48]. Similar to other large-scale neural network models, GCN tends to memorize parts of the training data including sensitive connections in its model weights, which could be extracted with sophisticated edge inference attacks, e.g., [21, 46, 50], leading to violations of privacy regulations such as GDPR [22] and CCPA [16].

Defending against such edge inference attacks is highly non-trivial, since the GCN training process is rather complex, and it is difficult to control what parts of the training data are memorized by the model. To address this issue, a rigorous solution is to train the GCN with edge differential privacy [13] (DP). As a classic privacy protection standard, DP has been widely accepted by both academia [14, 52] and industry [1, 34]. Edge DP, in particular, limits the adversary’s confidence in inferring the presence or absence of an edge by introducing random perturbations in the released GCN model weights, as elaborated in Section 2.3. Such random perturbations adversely impact model performance; hence, the main objective in this paper is to preserve the utility of the released GCN model, while satisfying the strong privacy requirement of edge DP.

In the literature, a typical mechanism for enforcing DP involves two key steps: (i) determining the *sensitivity* of the analysis result

to be released, and (ii) injecting calibrated random noise according to the result of (i) as well as the privacy parameters of DP, explained later in Section 2.3. In the context of GCN training with edge DP, the sensitivity is the maximum impact of adding or removing an edge in the input graph on the model weights, which, in general, is rather high. Specifically, as we explain in detail in Section 2.1, a GCN iteratively aggregates features from each node’s local neighborhood via its edges, and updates the node’s features with the aggregation results through graph convolution operations. Given an input graph  $G = \langle V, E \rangle$ , every edge  $e \in E$  can potentially have a significant impact on the result of a graph convolution operation, since the presence or absence of  $e$  may considerably alter the aggregation results for the two vertices connected by  $e$ . Moreover,  $e$  can have far-reaching effects as information gets further propagated from  $e$ ’s endpoints to other vertices in  $V$  in successive graph convolution operations. Consequently, training an effective GCN under edge DP is a highly challenging task, as the high sensitivity leads to heavy perturbations, and, thus, low model utility.

Although there exist DP algorithms for other types of neural network models, e.g., multi-layer perceptions [7], convolutional neural networks [2, 45], and complex architectures such as ResNet [12] and BERT [37], these solutions typically assume independence among individual training data records (e.g., an image or a textual document) in their sensitivity analysis. This is not the case for GCN training under edge DP, where the graph comprises interconnected vertex pairs via edges, which significantly complicates the sensitivity analysis. Consequently, it is unclear how to adapt generic solutions for deep learning with DP for our purpose.

Currently, there is only a limited collection of works on integrating DP with GCNs. Among these, DPGCN [46] injects random noise directly into the adjacency matrix of the input graph  $G$  to satisfy edge DP. As a result, every edge in  $G$  is perturbed with considerable probability (due to the high sensitivity with respect to an edge), which severely disrupts the message aggregation process among vertices in the GCN, leading to poor model utility as shown in our experiments in Section 6. A subsequent method LPGNet [28] attempts to mitigate this problem by iteratively refining and perturbing a smaller matrix that compresses the information of the original adjacency matrix. In another line of research, GAP [40] and ProGAP [39] introduce noise into the aggregated features after each round of message aggregation, instead of perturbing the adjacency matrix of  $G$ . As shown in our evaluation results, these methods achieve somewhat improved model utility compared to DPGCN; yet, their performance is still far lower than the non-private case, especially with more stringent privacy budget parameters.

**Our contributions.** We introduce graph convolutional networks via objective perturbation (GCON), a novel algorithm for training graph convolutional networks (GCNs) with differential privacy. The main idea of GCON is to view GCN training as an optimization problem and inject random noise into the corresponding objective function, as in the classic DPERM algorithm [7]. Unlike the existing solutions mentioned above, GCON maintains a complete and unaltered graph convolution process in GCNs, which avoids the problems of disrupted message aggregation encountered in existing solutions and the corresponding performance degradations.

Applying objective perturbation to GCN training is highly non-trivial. First, we face the challenge of how to effectively limit the sensitivity of GCN, i.e., the maximum impact of adding or removing an arbitrary edge on the GCN training objective. This problem is difficult in general, since each edge is involved in the GCN’s message aggregation process as described earlier. Fortunately, we found that the problem is tractable for certain flavors of GCNs that adopt an advanced aggregation scheme rooted in personalized PageRank (PPR), e.g., PPNP [27], detailed in Section 2.2. Unlike conventional message aggregation methods that iteratively multiply the adjacency matrix with the node feature matrix, PPNP controls the amount of information aggregated by each node from its neighbors, thereby effectively limiting information propagated through the edges, leading to reduced sensitivity. To further enhance our model’s accuracy under restrictive privacy constraints, we also adopt a variant of PPNP that uses an approximation of PPR, named APPR [27]. For both aggregation schemes, we derive tight, closed-form bounds on the sensitivity of the GCN training objective.

Another challenge for applying DPERM-style objective perturbation to GCN is the requirement for the objective function to exhibit convexity with respect to the model parameters. This is difficult for traditional GCNs with multiple layers and nonlinear activation functions between the layers, whose loss function is inherently non-convex. To address this issue, we follow the SGC approach (detailed in Section 2.2) that streamlines the GCN architecture by eliminating nonlinearities and consolidating parameter matrices between layers, transforming the GCN into a linear model. Previous research [20, 31, 47] has shown that GCN with SGC can still obtain high model utility. More importantly, we show that with SGC, the training objective of the GCN can be expressed as a convex optimization problem, making objective perturbation feasible.

Even with PPNP and SGC described above, the privacy analysis of GCN training is still a challenging task, due to the complex relationship between the sensitivity of aggregation, the injected noise, and the optimized output model parameters. To tackle this, we enhance the theoretical framework of DPERM with several fundamental results in Section 5. In particular, the added noise is carefully constructed by sampling from a multi-dimensional hypersphere whose radius follows the Erlang distribution, which is key to our privacy guarantee. Lastly, we employ an MLP-based feature encoder to deal with situations with high-dimensional features and/or few labeled vertices. To demonstrate the generalization capability and usability of our proposed model, we compare GCON on 4 real-world datasets with a range of homophily ratios against 6 baselines, under varying privacy budgets. The results demonstrate that GCON consistently and significantly outperforms existing solutions in accuracy across a broad spectrum of configurations.

In the following, Section 2 provides the necessary background on GCN and differential privacy. Section 3 clarifies our problem setting, while Section 4 presents the proposed solution GCON. Section 5 formally establishes the correctness of GCON and analyzes its privacy costs. Section 6 contains an extensive set of experiments. Section 7 overviews related work. Finally, Section 8 concludes the paper with directions for future work.

## 2 PRELIMINARIES

We use  $\|\mathbf{x}\|_2$  and  $\|\mathbf{x}\|_1$  to denote the  $\mathcal{L}_2$ -norm and  $\mathcal{L}_1$ -norm of a vector  $\mathbf{x}$ , respectively, and  $\|\mathbf{M}\|_F$  to denote the Frobenius norm of a matrix  $\mathbf{M}$ . In the following, Sections 2.1 and 2.2 present the general GCN concepts and two specific flavors of GCNs called SGC and PPNP, respectively. Section 2.3 presents the formal definition of differential privacy, as well as concepts related to the objective perturbation framework.

### 2.1 Graph Convolutional Networks

Graph Convolutional Networks (GCNs) [26] have emerged as a prominent neural network architecture for graph analytics. In what follows, we review the setup and basics of GCNs.

Consider an input graph with vertices  $V = \{1, 2, \dots, n\}$  and edges  $E$ . The edge set  $E$  is typically represented by an adjacency matrix  $\mathbf{A} \in \{0, 1\}^{n \times n}$ , where  $A_{ij} = 1$  signifies an edge from vertex  $i$  to vertex  $j$ . Let  $\mathbf{D}$  be a diagonal matrix where each diagonal element,  $D_{ii}$ , corresponds to the degree of vertex  $i$ . In GCNs, we often transform  $\mathbf{A}$  into a message passing matrix by multiplying the inverse of  $\mathbf{D}$  [8], written as  $\tilde{\mathbf{A}} = \mathbf{D}^{-1} \mathbf{A} \mathbf{D}$ ,  $r \in [0, 1]$ .

We present GCNs in the context of vertex classification. Specifically, each vertex  $v \in V$  is associated with a  $d_0$ -dimensional feature vector, as well as a  $c$ -dimensional one-hot label vector, i.e., if  $v$  belongs to the  $j$ -th class ( $1 \leq j \leq c$ ), then the  $j$ -th entry in the label vector is set to 1, and the remaining entries are set to 0. We denote  $\mathbf{X} \in \mathbb{R}^{n \times d_0}$  and  $\mathbf{Y} \in \mathbb{R}^{n \times c}$  as the feature matrix and label matrix of the  $n$  vertices, respectively.

An  $m$ -layer GCN iteratively computes the output of layer  $l$  ( $l = 1, 2, \dots, m$ ), denoted as  $Y^{(l)}$ , based on the message passing matrix  $\tilde{\mathbf{A}}$  and network parameter  $\{\Theta^{(l)}\}_{l=1}^m$ . In particular, we define  $Y^{(0)} = \mathbf{X}$ . At each layer  $l$ , the GCN aggregates the information of every node's neighbors by multiplying the normalized adjacency matrix  $\tilde{\mathbf{A}}$  with the preceding layer's output  $Y^{(l-1)}$ , and the corresponding layer's parameters  $\Theta^{(l)}$ . Formally, the GCN iteratively computes

$$Y^{(l)} = H_l \left( \tilde{\mathbf{A}} Y^{(l-1)} \Theta^{(l)} \right), \quad (1)$$

for  $l = 1, 2, \dots, m$ . Here  $H_l$  is some pre-defined activation function, e.g., the sigmoid function  $H_l(u) = 1/(1 + \exp(-u))$  or the linear mapping  $H_l(u) = u$ . The output of the last layer  $Y^{(m)}$  is regarded as the prediction for the vertices in the input graph, denoted as  $\hat{Y}$ .

**Training objective.** In a typical use case of GCN, a portion of the labels are used as the training set, say, with  $n_0 < n$  vertex labels. The training objective is to minimize the dissimilarity between the predicted labels and true labels of the labeled nodes in the training set by updating the network parameter  $\{\Theta^{(l)}\}_{l=1}^m$  (e.g., using stochastic gradient descent with backpropagation [4]). The dissimilarity is measured by the loss function, as follows:

$$L_\Lambda(\{\Theta^{(l)}\}_{l=1}^m; \hat{Y}, Y) = \frac{1}{n_0} \sum_i^{n_0} L(\{\Theta^{(l)}\}_{l=1}^m; \hat{\mathbf{y}}_i, \mathbf{y}_i) + \Lambda \sum_l^m \frac{1}{2} \|\Theta^{(l)}\|_F^2, \quad (2)$$

where  $\sum_l^m \frac{1}{2} \|\Theta^{(l)}\|_F^2$  is a regularization term for the network parameters,  $\Lambda$  is a hyperparameter, and the component  $L(\{\Theta^{(l)}\}_{l=1}^m; \hat{\mathbf{y}}_i, \mathbf{y}_i)$

is some function that evaluates the distance between the prediction  $\hat{\mathbf{y}}_i$  and the true label  $\mathbf{y}_i$  for node  $i$ , where the prediction  $\hat{y}$  is computed based on the network parameters  $\{\Theta^{(l)}\}_{l=1}^m$ .

### 2.2 SGC and PPNP

Next, we review two popular techniques, namely SGC and PPNP, which were proposed to improve GCN model performance in terms of both efficiency (e.g., memory consumption and computational cost in training and inference) and effectiveness (e.g., measured by prediction accuracy).

**SGC.** Simple Graph Convolution (SGC) [47] simplifies a multi-layer GCN by using a linear mapping, e.g.,  $H_l(u) = u$ , as the activation function in each graph convolution layer defined in Eq. (1). This leads to a streamlined GCN which still maintains an identical message propagation pathway as the original GCN. Formally, the model equation of an  $m$ -layer GCN is simplified to

$$\hat{Y} = Y^{(m)} = H(\tilde{\mathbf{A}}^m \mathbf{X} \Theta^{(1)} \Theta^{(2)} \dots \Theta^{(m)}) = H(\tilde{\mathbf{A}}^m \mathbf{X} \Theta), \quad (3)$$

where we have transformed the matrix product of  $\Theta^{(1)} \Theta^{(2)} \dots \Theta^{(m)}$  to a single matrix  $\Theta$  of dimension  $d_0 \times c$ . It has been demonstrated in [47] that SGC improves training efficiency while retaining the accuracy performance of the original GCN.

**PPNP.** Recall from Eq (1) that in each layer  $l$ , the traditional aggregation in GCN directly multiplies the previous output  $Y^{(l-1)}$  with the normalized adjacency matrix  $\tilde{\mathbf{A}}$ , which can be seen as the transition probability matrix in random walks [27]. PPNP [27] designs an advanced propagation scheme for improving the performance of GCNs, based on personalized PageRank (PPR) [35], instead of iteratively applying  $\tilde{\mathbf{A}}$  to aggregate features. In particular, PPR introduces the concept of restarting probability to a random walk. Let  $\mathbf{R}_0$  be an identity matrix  $\mathbf{I}$  denoting the roots. The PPR propagation matrix with  $m$  propagation steps, denoted as  $\mathbf{R}_m$ , is defined as

$$\mathbf{R}_m = (1 - \alpha) \tilde{\mathbf{A}} \mathbf{R}_{m-1} + \alpha \mathbf{I}, \quad (4)$$

where  $\alpha \in (0, 1]$  is the restart probability. When  $m$  approaches infinity,  $\mathbf{R}_m$  converges to  $\mathbf{R}_\infty$ , defined as

$$\mathbf{R}_\infty = \lim_{m \rightarrow \infty} \mathbf{R}_m = \alpha \left( \mathbf{I} - (1 - \alpha) \tilde{\mathbf{A}} \right)^{-1}. \quad (5)$$

PPNP initially processes  $\mathbf{X}$  through a feed-forward neural network  $M$  denoted as  $M(\mathbf{X})$ . Subsequently, it uses  $\mathbf{R}_\infty$  to aggregate the processed features  $M(\mathbf{X})$ . Formally, its model equation is

$$\hat{Y} = \mathbf{R}_\infty M(\mathbf{X}).$$

There remains an efficiency issue with the above approach: many real graphs are sparse, meaning that their message passing matrix  $\tilde{\mathbf{A}}$  is a sparse matrix; however, the inversion in Eq. (5) results in a  $n \times n$  dense matrix, leading to higher computational and memory costs. To address this issue, the authors of [27] further introduce an approximate version of PPR (APPR) to GCN, which employs  $\mathbf{R}_m$  with finite choices of  $m$ . In such cases, the corresponding propagation matrix is derived by expanding Eq. (4) from step  $m$  down to step 1, as follows:

$$\mathbf{R}_m = \alpha \sum_{i=0}^{m-1} (1 - \alpha)^i \tilde{\mathbf{A}}^i + (1 - \alpha)^m \tilde{\mathbf{A}}^m. \quad (6)$$

## 2.3 Differential Privacy

Differential privacy (DP) provides rigorous, information-theoretic privacy protection of individuals' private information. As mentioned in Section 1, DP ensures that an adversary can only infer with limited confidence the presence or absence of any individual of the input by observing the output. The most commonly used notion of DP is  $(\epsilon, \delta)$ -DP, defined as follows.

*Definition 2.1* ( $(\epsilon, \delta)$ -Differential Privacy (DP) [13]). A randomized algorithm  $\mathcal{A} : \mathcal{D} \rightarrow \mathcal{R}$  satisfies  $(\epsilon, \delta)$ -DP if given any neighboring datasets  $D, D' \subseteq \mathcal{D}$ , we have

$$\Pr[\mathcal{A}(D) \in \mathcal{O}] \leq \exp(\epsilon) \cdot \Pr[\mathcal{A}(D') \in \mathcal{O}] + \delta, \quad (7)$$

for any set of output  $\mathcal{O} \subseteq \mathcal{R}$ .

In Eq. (7), the *privacy budget*, specified by parameters  $\epsilon$  and  $\delta$ , quantifies the indistinguishability between the two distributions of  $\mathcal{A}(D)$  and  $\mathcal{A}(D')$  for any neighboring datasets  $D$  and  $D'$  (graphs in our setting). Smaller  $\epsilon$  and  $\delta$  indicate that the two distributions are more similar, which implies lower confidence for an adversary to infer a private edge (an edge in our case) of the input, and vice versa. In practice,  $\delta$  is usually set to a small value no more than the inverse of the dataset size (a special case is when  $\delta = 0$ , which is referred to as  $\epsilon$ -DP), and  $\epsilon$  is often used to control the strength of the privacy requirement. The above definition involves the concept of neighboring datasets, whose generic definition is as follows.

*Definition 2.2* (Neighboring datasets). Two datasets  $D$  and  $D'$  are defined as *neighboring datasets* if they differ by one record.

The above generic definition involves two abstract concepts, *dataset* and *record*. In the context of graph analytics, a common notion is *edge DP* [28, 39, 40], in which the entire input graph  $G = \langle V, E \rangle$  is considered a dataset, and an edge  $e \in E$  is considered a record, i.e., two neighboring graphs  $G$  and  $G'$  differ by exactly one edge. In this paper, we aim to satisfy edge-DP in the training and release of a GCN model.

This paper involves a variant of  $(\epsilon, \delta)$ -DP,  $(\epsilon, \delta)$ -Probabilistic Differential Privacy (pDP), which can be converted to  $(\epsilon, \delta)$ -DP. Its formal definition is described in Appendix B.1.

As described in Section 1, the proposed solution is based on the general framework of objective perturbation, first introduced in DPERM [7]. The main idea is that to release a trained machine learning model, we randomly perturb its training objective function to satisfy DP; note that the objective function covers the underlying training dataset. Then, model fitting can be performed with an arbitrary optimization algorithm, based on the noisy objective function. This framework requires that the objective function to be strongly convex and have bounded derivatives with respect to the model weights. The concept of strong convexity is defined as follows.

*Definition 2.3* (Convex and strictly convex). A function  $F : \mathbb{R}^{d_1 \times d_2} \rightarrow \mathbb{R}$  is convex if  $\forall \Theta_1, \Theta_2 \in \mathbb{R}^{d_1 \times d_2}$  and  $\forall \alpha \in (0, 1)$ , we have

$$F(\alpha\Theta_1 + (1 - \alpha)\Theta_2) \leq \alpha F(\Theta_1) + (1 - \alpha)F(\Theta_2)$$

In particular,  $F$  is strictly convex if  $\forall \Theta_1, \Theta_2 \in \mathbb{R}^{d_1 \times d_2}$ ,  $\Theta_1 \neq \Theta_2$  and  $\forall \alpha \in (0, 1)$ , we have

$$F(\alpha\Theta_1 + (1 - \alpha)\Theta_2) < \alpha F(\Theta_1) + (1 - \alpha)F(\Theta_2)$$

*Definition 2.4* (Strongly convex). A function  $F(\Theta)$  over  $\Theta \in \mathbb{R}^{d_1 \times d_2}$  is strongly convex if  $\exists \lambda > 0$ ,  $F(\Theta) - \lambda \|\Theta\|_F^2$  is convex.

FACT 1. Consider any  $\Lambda > 0$ .  $\Lambda \|\Theta\|_F^2$  is strongly convex. In addition, if  $F(\Theta)$  is convex, then  $F(\Theta) + \Lambda \|\Theta\|_F^2$  is strongly convex.

## 3 PROBLEM SETTING

Our goal is to design an effective algorithm for training GCNs with differential privacy. In our presentation, we focus on vertex classification as described in Section 2.1; other applications of GCN are left as future work. In particular, the algorithm takes a graph  $G = \langle V, E \rangle$  with vertex set  $V$  and edge set  $E$ , as well as features  $X$  and labels  $Y$  of the vertices. It outputs GCN parameters  $\Theta$ .

In terms of privacy, we focus on edge DP as described in Section 2.3, which prevent an adversary from differentiating between any two neighboring graphs that differ by a single edge. We consider the vertex set  $V$  as well as features/labels of vertices in the training set as public information.

Formally, for any graph dataset  $D = \langle V, E, X, Y \rangle$  (which consists of vertex set  $V$ , edge set  $E$ , feature matrix  $X$ , and label matrix  $Y$ ) and its edge-level neighboring dataset  $D' = \langle V, E', X, Y \rangle$  whose edge set  $E'$  differs from  $E$  by exactly one edge, the output  $\Theta$  of algorithm  $\mathcal{A}$  satisfies

$$\Pr[\mathcal{A}(V, X, Y, E) \in \mathcal{O}] \leq e^\epsilon \Pr[\mathcal{A}(V, X, Y, E') \in \mathcal{O}] + \delta, \quad (8)$$

## 4 GCON

### 4.1 High-Level Idea and Major Challenges

In a nutshell, the main idea of the proposed GCON algorithm is to inject random noise into the objective function of GCN training, following the DPERM framework described towards the end of Section 2.3. The scale of noise is carefully calibrated to satisfy edge DP with given privacy parameters  $\epsilon$  and  $\delta$ . Note that GCON does not directly perturb the graph topology, nor does it introduce additional noise during the training process besides objective perturbation. This way, GCON avoids the severe disruption of the GCN's message propagation/aggregation process commonly encountered in existing solutions, as explained in Section 1.

Realizing this idea involves overcoming several major challenges:

**Challenge 1: bounding the sensitivity of GCN's training objective.** Since the added noise required to satisfy edge DP is calibrated based on the sensitivity of the GCN training objective with respect to the presence/absence of an edge, it is crucial to derive a tight upper bound of this sensitivity. This is challenging since an edge can not only affect the message passing of its endpoints but also vertices further away due to multiple propagations in the GCN. Specifically, according to Eq. (1), traditional GCNs iteratively multiply the normalized adjacency matrix with the nodes' representations. With sufficient iterations, features from all reachable vertices are aggregated. In the worst case, a single edge can have a drastic effect on the connectivity of the vertices. Consequently, it is difficult to bound its impact on the GCN's predictions, and, thus, the objective function defined in Eq. (2).

**Challenge 2: ensuring strong convexity of the GCN training objective.** As described in Section 2.3, the objective perturbation scheme, according to DPERM, relies on two crucial properties of the

objective function: strong convexity (Definition 2.4) and bounded derivatives with respect to the model parameters. Both are rather difficult for traditional GCNs that involve multiple layers with non-linear activation functions between the layers.

**Challenge 3: quantifying the impact of noise.** For the purpose of privacy analysis, we need to quantify the impact that the noise injected into the objective function on the (distribution of) optimal model parameters. The quantification involves analyzing the Jacobian matrices of the mapping from the parameters to the noise. In the original derivation of DPERM [7], the focus is on isolating a single divergent element within the Jacobian matrices. However, this approach is inadequate for training GCNs, where the Jacobian matrices differ in numerous items.

In addition to the above major challenges, we also face the issue that the feature dimensionality  $d$  and the number of labeled nodes  $n_0$  of the training dataset (explained in Section 2.1) could significantly affect the privacy guarantee. In particular, a larger  $d$  corresponds to more model parameters, which may lead to more leakage of sensitive information. Meanwhile, when  $n_0$  is much smaller than the total number of vertices  $n$ , which is often the case in real applications where labeling is expensive, the addition or removal of a single edge connecting two labeled vertices on the trained model, which leads to higher sensitivity, heavier perturbations to satisfy edge DP, and lower model utility. In the next subsection, we present an overview of the proposed solution GCON, focusing on addressing the above challenges.

## 4.2 Solution Overview

For Challenge 1, to control the sensitivity, we follow the PPNP approach (described in Section 2.2) that utilizes personalized PageRank propagation (PPR). This scheme has two nice properties: (i) a stationary state of the propagation matrix, which means the sensitivity can be bounded, and (ii) a tunable restart probability  $\alpha$ , which we can modulate the extent of each node’s influence over its neighbors. For instance, at  $\alpha = 1$ , nodes propagate nothing to their neighbors; conversely, at  $\alpha = 0$ , the scheme reverts to the standard propagation mechanism employed in conventional GCNs. The sensitivity of the objective function can be further reduced by employing APPR instead of PPR, as in PPNP. Later, we present the detailed construction of PPR and APPR propagation matrices in Section 4.3.2, and derive tight, closed-form bounds on the sensitivity of the GCN objective function in Lemma 5.3.

For Challenge 2, we make the GCN objective function strong convex using the idea of SGC (explained in Section 2.2), which simplifies the GCN network with linear activations. SGC has been shown to be effective in various non-DP settings [20, 31], and the fact that it enables the objective perturbation approach with much reduced perturbations more than compensates for its loss of accuracy performance due to use of the linear activations. The detailed SGC-based model architecture is presented later in Section 4.3.3.

Regarding Challenge 3, we establish a connection between the sensitivity of the aggregate features, the additive noise, and the optimal output network parameters through a careful theoretical analysis in Section 5. The underlying principle is that the probability density of the optimal output is correlated with both the noise density and the determinant of the Jacobian matrix of mapping

from the network parameters to the additive noise (according to probability theory [6]). We employ a specific noise distribution, named Erlang-Normal distribution (detailed in Algorithm 2), to facilitate the analysis of noise density. Further, it is also challenging to bound the ratio of determinants of two Jacobian matrices on two neighboring graphs. To address this, we present several useful lemmas, which might be of independent interest.

Finally, to address the issue that the feature dimensionality  $d$  and the label vertices cardinality  $n_0$  significantly affect the privacy guarantees, we present an MLP-based feature encoder, detailed in Section 4.3.1, which maps the features to a lower-dimensional space and assign pseudo labels to unlabeled nodes.

## 4.3 Detailed GCON Algorithm

**4.3.1 Feature Encoder.** First, we propose a feature encoder based on multilayer perceptron (MLP) to expand the training set size and reduce feature dimension. Let the feature matrix of the labeled and unlabeled vertices be  $X_l \in \mathbb{R}^{n_0 \times d_0}$  and  $X_{ul} \in \mathbb{R}^{(n-n_0) \times d_0}$ , respectively. The framework of our encoder is as follows.

$$\begin{aligned}\bar{X}_l &= H_{mlp}(MLP(X_l; \mathbf{W}_1)), \\ \bar{Y}_l &= H(\bar{X}_l \mathbf{W}_2),\end{aligned}$$

where  $\mathbf{W}_1$  and  $\mathbf{W}_2$  are model parameters and  $H_{mlp}$  and  $H$  are activation functions. Note that in our encoder, we exclusively utilize vertex features and labels, which are deemed non-private in our problem setting defined in Section 3. The encoder operates by initially transforming the original features  $X_l$  into a new feature space, resulting in  $\bar{X}_l \in \mathbb{R}^{n_0 \times d_1}$ , where  $d_1$  is the new dimension. After this transformation, the encoder predicts the labels of these features, represented as  $\bar{Y}_l$ . Let the real label matrix of  $X_l$  and  $X_{ul}$  be  $Y_l$  and  $Y_{ul}$  ( $Y_{ul}$  is unknown in training), respectively. The training of the encoder is carried out through the minimization of a classification loss function  $L_{mlp}$  as follows.

$$\mathbf{W}_1^*, \mathbf{W}_2^* = \underset{\mathbf{W}_1, \mathbf{W}_2}{\operatorname{argmin}} L_{mlp}(\bar{Y}_l, Y_l).$$

Upon completion of the training, we encode all node features  $X$  to new features  $\bar{X} \in \mathbb{R}^{n \times d_1}$  by  $\mathbf{W}_1^*$  as follows.

$$\bar{X} = H_{mlp}(MLP(X; \mathbf{W}_1^*)).$$

Further, we assign pseudo-labels  $\bar{Y}_{ul}$  to the unlabeled vertices through  $\mathbf{W}_2^*$ , as follows.

$$\bar{Y}_{ul} = H(\bar{X}_{ul} \mathbf{W}_2^*),$$

where each element of  $\bar{Y}_{ul}$  locates in  $[0, 1]$  through  $H$  (e.g., setting  $H$  as the softmax activation). Finally, we can extend the labels from  $Y_l$  to  $\bar{Y} = Y_l \cup \bar{Y}_{ul}$ , i.e., can increase the number of labeled vertices  $n_0$  to  $n_1 \in [n_0, n]$ . The complete algorithm of the encoder is outlined in Algorithm 4 in Appendix D. Note that the encoder does not involve any private edge information, and, thus, preserves edge privacy automatically.

For simplicity, in the following sections, we use  $X \in \mathbb{R}^{n \times d_1}$  and  $Y \in \mathbb{R}^{n \times c}$  to denote the feature matrix and the label matrix, respectively, instead of  $\bar{X}$  and  $\bar{Y}$ .

**4.3.2 Propagation with PPR and APPR.** We employ two advanced propagation schemes in GCON, PPR and APPR. Let  $\hat{\mathbf{A}} = \mathbf{A} + \mathbf{I}$  be the adjacency matrix with self-loops. Let  $\mathbf{D}$  be the diagonal degree matrix of  $\hat{\mathbf{A}}$ , i.e.,  $D_{ii} = \sum_k \hat{A}_{ik}$  and  $D_{ij} = 0$  for  $i \neq j$ . We follow the normalization for  $\hat{\mathbf{A}}$  in [8] that sets  $\tilde{\mathbf{A}} = \mathbf{D}^{r-1} \hat{\mathbf{A}} \mathbf{D}^{-r}$  where  $r \in [0, 1]$ . In this work we set  $r = 0$  and obtain  $\tilde{\mathbf{A}} = \mathbf{D}^{-1} \hat{\mathbf{A}}$ . Given  $\tilde{\mathbf{A}}$ , we construct our propagation matrix  $\mathbf{R}_m$ ,  $m \in [0, \infty]$ , utilizing the PPR and APPR schemes (Eq. (5) & (6)), as follows.

$$\mathbf{R}_m = \begin{cases} \mathbf{I}, & m = 0, \\ \alpha \sum_{i=0}^{m-1} (1-\alpha)^i \tilde{\mathbf{A}}^i + (1-\alpha)^m \tilde{\mathbf{A}}^m, & m \in (0, \infty) \\ \alpha \left( \mathbf{I} - (1-\alpha) \tilde{\mathbf{A}} \right)^{-1}, & m = \infty \end{cases} \quad (9)$$

In the above equation,  $\mathbf{R}_\infty$  and  $\mathbf{R}_m$ , with  $m \in (0, \infty)$ , represent the PPR and APPR schemes, respectively. For simplicity, we no longer emphasize which specific scheme GCON uses unless necessary. Instead, we represent both schemes with  $\mathbf{R}_m$ , where  $m$  ranges from 0 to  $\infty$ . We prove that the matrix  $\mathbf{I} - (1-\alpha)\tilde{\mathbf{A}}$  always has an inverse in Lemma A.1 in Appendix A.1.

**4.3.3 SGC-Based Network Architecture.** In the step of message propagation, we multiply our propagation matrix  $\mathbf{R}_m$  with the feature matrix  $\mathbf{X}$  and obtain the aggregate feature matrix

$$\mathbf{Z}_m = \mathbf{R}_m \mathbf{X}. \quad (10)$$

Furthermore, to enhance the model performance, we augment the features by using several different propagation steps  $m_1, m_2, \dots, m_s \in [0, \infty]$  and concatenating them as

$$\mathbf{Z} = \frac{1}{s} (\mathbf{Z}_{m_1} \oplus \mathbf{Z}_{m_2} \oplus \dots \oplus \mathbf{Z}_{m_s}), \quad (11)$$

where  $\oplus$  represents concatenation by row. We weight the concatenated features by  $\frac{1}{s}$  to bound the  $L_2$ -norm of each row of  $\mathbf{Z}$ . We then input  $\mathbf{Z}$  into our GCN.

For the network architecture, we follow SGC idea (outlined in Section 2.2) and build a single-layer network with linear mapping. Let  $\Theta \in \mathbb{R}^{d \times c}$  be the 1-layer network parameters, where  $d = sd_1$ . Formally, the model makes prediction  $\hat{\mathbf{Y}}$  by computing  $\hat{\mathbf{Y}} = \mathbf{Z}\Theta$ .

**4.3.4 Strongly-Convex Loss Function.** The formulation of the original loss function  $L_\Lambda(\Theta; \mathbf{Z}, \mathbf{Y})$  is shown in Eq. (2). Let  $\mathbf{z}_i$  and  $\hat{\mathbf{y}}_i$  denote the  $i$ -th columns of  $\mathbf{Z}^T$  and  $\hat{\mathbf{Y}}^T$ , respectively. In Eq. (2), for the convenience of subsequent analysis, we define  $L(\Theta; \mathbf{y}_i, \mathbf{y}_i)$  as either the MultiLabel Soft Margin Loss [36] or the pseudo-Huber Loss [43], both of which are convex w.r.t.  $\Theta$ . As in our solution,  $\hat{\mathbf{y}}_i$  is obtained by  $\mathbf{Z}$  and  $\Theta$ , here we denote it as  $L(\Theta; \mathbf{z}_i, \mathbf{y}_i)$ . Both loss functions evaluate and sum the discrepancies between each element of  $\mathbf{y}_i$  (denoted as  $\mathbf{y}_{ij}$ ,  $j \in [1, c]$ ) and its corresponding prediction,  $\mathbf{z}_i^T \theta_j$ , where  $\theta_j$  is the  $j$ -th column of  $\Theta$ . Formally,

$$L(\Theta; \mathbf{z}_i, \mathbf{y}_i) = \sum_j^c \ell(\mathbf{z}_i^T \theta_j; \mathbf{y}_{ij}), \quad (12)$$

In MultiLabel Soft Margin Loss,  $l$  is defined as

$$\ell(x; y) = -\frac{1}{c} \left( y \log\left(\frac{1}{1+e^{-x}}\right) + (1-y) \log\left(\frac{e^{-x}}{1+e^{-x}}\right) \right), \quad (13)$$

In pseudo-Huber Loss,  $l$  is defined as

$$\ell(x; y) = \frac{\delta_l^2}{c} \left( \sqrt{1 + \frac{(x-y)^2}{\delta_l^2}} - 1 \right), \quad (14)$$

where the weight  $\delta_l$  is a hyperparameter.

Under the above setting,  $L_\Lambda(\Theta; \mathbf{Z}, \mathbf{Y})$  is strongly convex w.r.t.  $\Theta$  (formally proved in Lemma A.2 in Appendix A.2), which is essential for our subsequent privacy analysis.

**4.3.5 Objective Perturbation.** Next, we perturb the above strongly convex loss function to satisfy edge DP. Formally, the noisy loss function  $L_{priv}(\Theta; \mathbf{Z}, \mathbf{Y})$  is

$$\begin{aligned} L_{priv}(\Theta; \mathbf{Z}, \mathbf{Y}) &= L_\Lambda(\Theta; \mathbf{Z}, \mathbf{Y}) + \frac{1}{n_1} \mathbf{B} \odot \Theta + \frac{1}{2} \Lambda' \|\Theta\|_F^2 \\ &= \frac{1}{n_1} \sum_i^{n_1} L(\Theta; \mathbf{z}_i, \mathbf{y}_i) + \frac{1}{2} \Lambda \|\Theta\|_F^2 + \frac{1}{n_1} \mathbf{B} \odot \Theta + \frac{1}{2} \Lambda' \|\Theta\|_F^2, \end{aligned} \quad (15)$$

where  $\Lambda'$  is a parameter computed by Eq. (25) (detailed later in Section 5),  $\odot$  denotes an element-wise product followed by a summation of the resulting elements, and  $\mathbf{B} = (\mathbf{b}_1, \mathbf{b}_2, \dots, \mathbf{b}_c)$  is a noise matrix. The columns  $\mathbf{b}_1, \mathbf{b}_2, \dots, \mathbf{b}_c$  of  $\mathbf{B}$  are independently and uniformly sampled on a  $d$ -dimensional sphere with a radius following the Erlang distribution whose probability density function (PDF) is

$$\gamma(x) = \frac{x^{d-1} e^{-\beta x} \beta^d}{(d-1)!}. \quad (16)$$

In the above equation,  $\beta$  is a parameter computed by Eq. (26) (detailed later in Section 5).

We minimize  $L_{priv}(\Theta; \mathbf{Z}, \mathbf{Y})$  to obtain the network  $\Theta_{priv}$ , which is released to the analyst/adversary. Formally,

$$\Theta_{priv} = \underset{\Theta}{\operatorname{argmin}} L_{priv}(\Theta; \mathbf{Z}, \mathbf{Y}). \quad (17)$$

**4.3.6 Inference.** We then utilize the obtained network  $\Theta_{priv}$  to perform inference for the target unlabeled vertices. We consider the setup where the server publishes the trained model and then an untrusted user, represented as an unlabeled vertex within the target vertices, queries the model and receives the predicted label. The target vertices might belong to either (i) the same graph as the training data or (ii) a different graph with possibly DP requirement.

We focus on scenario (i) in our evaluation as it is the standard evaluation setup in the literature [28, 39, 40]. As the untrusted user knows her/his edge information, we do not add noise when utilizing the information of her/his direct neighbors, while edges other than its own are private. Accordingly, we devise an inference approach that aggregates the features of directly connected vertices and generates predictions  $\hat{\mathbf{Y}}$ , as shown in Eq. (18), where  $\alpha_l$  is a hyperparameter ranging in  $[0, 1]$  (the restart probability at the inference stage). Note that this approach involves only the edges directly connected to the query vertex, which are assumed to be known to the untrusted user, and no other edges in the graph. Hence, this approach satisfies edge DP as it does not reveal any additional private edge information of non-neighboring vertices to

---

**Algorithm 1:** The training algorithm for GCON

---

**Input:** Training dataset  $D = \{V, E, A, X, Y\}$ , new feature dimension  $d_1$ , loss function  $\ell$ , restart probability  $\alpha$ , propagation steps  $m_1, m_2, \dots, m_s$ , regularization coefficient  $\Lambda$ , privacy parameters  $\epsilon_0, \delta$ , and budget allocator  $\omega$ .

**Output:** Approximate minimizer  $\Theta_{priv}$ .

- 1  $X, Y = \text{FeatureEncoder}(X, Y, d_1)$ ;
  - 2 Initialize model parameters  $\Theta$ ;
  - 3  $\tilde{A} = \mathbf{D}^{-1}(A + I)$ ;
  - 4 Compute  $R_{m_1}, R_{m_2}, \dots, R_{m_s}$  by Eq. (9);
  - 5 Compute  $Z_{m_1}, Z_{m_2}, \dots, Z_{m_s}$  by Eq. (10);
  - 6  $Z = \frac{1}{s}(Z_{m_1}, Z_{m_2}, \dots, Z_{m_s})$ ;
  - 7 Compute  $\Lambda'$ , and  $\beta$  by Eq. (25) and (26);
  - 8 Construct  $B$ , whose columns  $b_1, b_2, \dots, b_c$  are independently drawing by Algorithm 2 with inputs  $d, \beta$ ;
  - 9 Construct  $L_{priv}$  by Eq. (15);
  - 10  $\Theta_{priv} = \text{argmin } L_{priv}$ ;
  - 11 **return**  $\Theta_{priv}$ ;
- 

the querying vertex.

$$\hat{R}_{m_i} = \begin{cases} I, & m_i = 0 \\ (1 - \alpha_I)\tilde{A} + \alpha_I I, & m_i > 0 \end{cases} \quad i \in [1, s] \quad (18)$$
$$\hat{Y} = (\hat{R}_{m_1}X \oplus \hat{R}_{m_2}X \oplus \dots \oplus \hat{R}_{m_s}X)\Theta_{priv}$$

In scenario (ii), if the edges in the different graph are private, we employ the same inference approach as in Eq. (18). If the edges are public, we can directly compute  $Z$  without a DP mechanism, and derive labels by  $\hat{Y} = Z\Theta_{priv}$ . We present the corresponding procedure as in Algorithm 3.

#### 4.4 The Complete Algorithm

The complete training algorithm of GCON is shown in Algorithm 1. In the input,  $\epsilon_0$  and  $\delta$  represent the privacy constraints;  $d_1, \alpha, \{m_i\}_{i=1}^s$ , and  $\Lambda$  are tunable hyperparameters. In Line 1, we preprocess the feature matrix  $X$  and label matrix  $Y$  by the feature encoder presented in Section 4.3.1. In Lines 4-5, we construct the propagation matrices  $\{R_{m_i}\}_{i=1}^s$  and  $\{Z_{m_i}\}_{i=1}^s$ . In Line 6, we construct the augmented feature matrix  $Z$ . In Line 7, we compute  $\Lambda'$  and  $\beta$ , which sets up the stage for the objective perturbation (the detailed computations are explained in Section 5). In Line 8, we sample the perturbation noise by running Algorithm 2. In Line 9, we construct the noisy objective function, based on the sampled noise. In Line 10, we minimize the objective function and obtain the optimal network parameters.

Algorithm 2 first samples the radius  $a$  from the Erlang distribution (Eq. (16)) that has been implemented in many popular libraries [43]. To sample each direction in the hypersphere with equal probability, we then sample a vector  $u$  from a  $d$ -dimensional normal distribution and scale its length to  $a$ . The correctness of Algorithm 2 is explained in Appendix A.3.

## 5 ANALYSIS

In this section, we show that GCON (Algorithm 1) satisfies  $(\epsilon, \delta)$ -DP with specific input parameters, formalized in Theorem 5.1.

---

**Algorithm 2:** Noise sampling

---

**Input:** Dimension  $d$ , distribution parameter  $\beta$

**Output:** Vector  $b_1$  with dimension  $d$

- 1 Sample  $a \in (0, +\infty)$  with a PDF shown in Eq. (16);
  - 2 Sample  $u_1, \dots, u_d$  independently according to the normal distribution  $\mathcal{N}(0, 1)$ ;
  - 3 **for**  $i \in [1, d]$  **do**
  - 4      $b_{1,i} \leftarrow au_i / \sqrt{u_1^2 + \dots + u_d^2}$
  - 5  $b_1 = (b_{1,1}, \dots, b_{1,d})$ ;
  - 6 **return**  $b_1$ ;
- 

---

**Algorithm 3:** The inference algorithm for GCON

---

**Input:** Optimized model  $\Theta_{priv}$ , target dataset  $D = \{V, E, A, X, Y\}$ , propagation steps  $m_1, m_2, \dots, m_s$ , and  $\alpha_I$ .

**Output:** Label predictions  $\hat{Y}$ .

- 1 **if** *private inference* **then**
  - 2     **for**  $i \in [1, s]$  **do**
  - 3          $\hat{R}_{m_i} = \begin{cases} I, & m_i = 0 \\ (1 - \alpha_I)\tilde{A} + \alpha_I I, & m_i > 0 \end{cases}$
  - 4      $\hat{Y} = (\hat{R}_{m_1}X \oplus \hat{R}_{m_2}X \oplus \dots \oplus \hat{R}_{m_s}X)\Theta_{priv}$ ;
  - 5 **else**
  - 6     Compute  $Z$  by Eq. (11) on  $D$ ;
  - 7      $\hat{Y} = Z\Theta_{priv}$ ;
  - 8 **return**  $\hat{Y}$ ;
- 

**THEOREM 5.1.** *Algorithm 1 satisfies  $(\epsilon, \delta)$ -pDP and  $(\epsilon, \delta)$ -DP, with inputs including  $n_1, c, d, \ell(x; y), \alpha, \Lambda, \omega, \{m_i\}_{i=1}^s$ , and parameters set to be Eq. (19)-(26).*

$$c_1 = \sup(|\ell'|), c_2 = \sup(|\ell''|), c_3 = \sup(|\ell'''|). \quad (19)$$

$$c_{sf} = \min\{u \text{ s.t. } u > 0 \text{ and } \int_0^u \frac{x^{d-1}e^{-x}}{(d-1)!} dx \geq 1 - \frac{\delta}{c}\}. \quad (20)$$

$$\Psi(Z) = \frac{1}{s} \sum_i \frac{2(1-\alpha)}{\alpha} [1 - (1-\alpha)^{m_i}]. \quad (21)$$

$$\Lambda = \max\left(\Lambda, \frac{cc_2\Psi(Z)c_{sf}}{n_1\omega\epsilon} + \xi\right), \xi \in \mathbb{R}^+. \quad (22)$$

$$c_\theta = \frac{n_1\omega\epsilon c_1 + cc_1\Psi(Z)c_{sf}}{n_1\omega\epsilon\Lambda - cc_2\Psi(Z)c_{sf}}. \quad (23)$$

$$\epsilon_\Lambda = cd \log\left(1 + \frac{(2c_2 + c_3c_\theta)\Psi(Z)}{dn_1\Lambda}\right). \quad (24)$$

$$\Lambda' = \begin{cases} 0, & \text{if } \epsilon_\Lambda \leq (1-\omega)\epsilon \\ \frac{c(2c_2+c_3c_\theta)\Psi(Z)}{n_1(1-\omega)\epsilon} - \Lambda, & \text{otherwise.} \end{cases} \quad (25)$$

$$\beta = \frac{\max(\epsilon - \epsilon_\Lambda, \omega\epsilon)}{c(c_1 + c_2c_\theta)\Psi(Z)}. \quad (26)$$

### 5.1 Analysis Overview

Our proof has two primary stages: (i) quantifying the sensitivities of the PPR/APPR aggregate matrix  $Z_m$  (Eq. (10)) and the concatenate feature matrix  $Z$  (Eq. (11)), and (ii) based on the findings from (i), quantifying the correlation between the noise  $B$  and the optimally

derived network parameters  $\Theta_{priv}$ . For stage (i), our analysis starts with the sensitivity of the normalized adjacency matrix  $\tilde{A}$ , and progressively extends to  $\tilde{A}^m$ ,  $R_m$ ,  $Z_m$ , and  $Z$ . Adding or removing one edge alters two elements in  $\tilde{A}$  ( $A$  is symmetric). Leveraging several pivotal properties of  $\tilde{A}^m$  (presented in Lemma 5.4), we employ mathematical induction to bound the sensitivities of  $\tilde{A}$ ,  $\tilde{A}^2, \dots, \tilde{A}^m$ , and their linear combinations  $R_m$  (we analyze the special case  $R_\infty$  separately). Given that the feature matrix  $X$  remains constant across edge-level neighboring graphs, the sensitivity of  $Z_m$  is inferred through standard matrix multiplications. Lastly, by summing the sensitivities of  $\{Z_m\}_{i=1}^s$ , we obtain the sensitivity of  $Z$ , which is evaluated by  $\sum_i^n \|z_i - z'_i\|_2$ , as defined in Definition 5.2.

For stage (ii), it has been demonstrated in DPERM [7] that, given graphs  $G$  and  $G'$ , the ratio of the densities of two optimal network parameters  $\Theta_{priv}$  and  $\Theta'_{priv}$  is proportional to the ratio of densities  $\frac{\mu(B|G)}{\mu(B'|G')}$  of two corresponding noises  $B$  and  $B'$ , and inversely proportional to the ratio of the determinants of the respective Jacobian matrices  $J(\Theta_{priv} \rightarrow B|G)$  and  $J(\Theta'_{priv} \rightarrow B'|G')$ . Our sampling method, detailed in Algorithm 2, ensures that each column  $b_j$  of  $B$  is independent of the other columns. Similarly, the derivative of each column  $\theta_j$  of  $\Theta_{priv}$  is independent of those of the other columns in the context of the perturbed loss function  $L_{priv}$  as specified in Section 4.3.5. Hence, we focus on examining the ratios of densities of noises  $\frac{\mu(b_j|G)}{\mu(b'_j|G')}$  and the ratios of determinants of the Jacobian matrices  $|\frac{\det(J(\theta_j \rightarrow b'_j|G'))}{\det(J(\theta_j \rightarrow b_j|G))}|$  (denoted as  $|\frac{\det(J')}{\det(J)}|$ ), for all  $j \in [1, c]$ .

The ratio  $\frac{\mu(b_j|G)}{\mu(b'_j|G')}$  can be bounded by a meticulously chosen parameter  $\beta$ . For the latter, the ratio of determinants of two matrices satisfies  $|\frac{\det(J')}{\det(J)}| = |\det(J'J^{-1})|$ . Given that the determinant of a matrix is equivalent to the product of its singular values, our analysis shifts focus to examining the singular values of  $J'J^{-1}$ . By applying the Courant–Fischer min-max theorem [10], we bound each singular value of  $J'J^{-1}$  through the product of the respective singular values of  $J'$  and  $J^{-1}$ . The singular values of  $J^{-1}$  are the reciprocals of the singular values of  $J$ . The mapping  $\Theta_{priv} \rightarrow B|G$  and  $\Theta'_{priv} \rightarrow B'|G'$  are constituted by the loss function, which aggregates the loss for features  $z_i$  and  $z'_i$  respectively. Corollary 3.4.3 in [23] indicates that the sum of singular values of a matrix resulting from addition is less than the sum of the singular values of each individual matrix. Consequently, we decompose the Jacobian matrix into a summation of  $n_1$  matrices, each associated with  $z_i$  or  $z'_i$ , and analyze their respective singular values utilizing Corollary 3.4.3 in [23]. The discrepancy in singular values of matrices associated with  $z_i$  and  $z'_i$  is quantifiable through  $\|z_i - z'_i\|_2$ . Ultimately, we link the sum of these singular values to the previously established sensitivity of  $Z$ , enabling us to derive  $|\frac{\det(J')}{\det(J)}|$ .

In the following, we provide a detailed analysis of the sensitivities of  $Z_m$  and  $Z$  in Section 5.2, which forms a foundational component of the theorem’s proof, summarized in Section 5.3. Supporting lemmas along with their proofs are included in Appendices A.5–B.3.

## 5.2 Sensitivities of $Z_m$ and $Z$

We define the sensitivities of  $Z_m$  and  $Z$  by Definition 5.2, denoted as  $\psi(Z_m)$  and  $\psi(Z)$ , respectively. Since  $Z$  is simply a concatenation of  $Z_m$ , the difficulty and focus of sensitivity analysis lie on  $Z_m$ . The bounds of  $\psi(Z_m)$  and  $\psi(Z)$  are established in Lemma 5.3. Lemma 5.3 elucidates the correlations of the sensitivity of  $Z_m$  with two key factors: the propagation step  $m$  and the restart probability  $\alpha$ . The rationale behind these correlations is as follows. Firstly, a larger propagation step  $m$ , results in each node disseminating its features to a more expansive neighborhood, thereby amplifying the sensitivity. Secondly, a smaller value of  $\alpha$  leads to each step of the propagation matrix incorporating more information from the edges (indicated by  $(1 - \alpha) \cdot \tilde{A}$ ). This elevates the influence of individual edges within the graph, thereby increasing the sensitivity.

These correlations provide valuable insights for managing sensitivity within the PPR/APPR schemes, which are advantageous in practice. These insights reveal a trade-off: balancing the amount of sensitivity, which directly influences the amount of additional noise needed for privacy protection, against the efficacy of the propagation matrix. For instance, in practical scenarios constrained by limited privacy budgets, opting for a smaller propagation step  $m$  or a larger restart probability  $\alpha$  can reduce the sensitivity. This reduction, in turn, diminishes the additional noise, thereby offering a pathway to enhance the model’s performance.

*Definition 5.2 (Sensitivity metric  $\psi$ ).* Given a graph  $G$ , let  $G'$  be any of its edge-level neighboring graphs. Let  $Z$  and  $Z'$  be two matrices computed in the same way (e.g., by Eq. (10) or (11)) on  $G$  and  $G'$ , respectively. Let  $z_i$  and  $z'_i$  denote the  $i$ -th rows of  $Z$  and  $Z'$ , respectively. The sensitivity of  $Z$  is defined by

$$\psi(Z) \triangleq \sum_{i=1}^n \|z'_i - z_i\|_2.$$

LEMMA 5.3. For  $Z_m$  computed by Eq. (10), we have

$$\psi(Z_m) \leq \frac{2(1 - \alpha)}{\alpha} [1 - (1 - \alpha)^m] \triangleq \Psi(Z_m), \quad (27)$$

where  $\psi$  is defined in Definition 5.2. Specifically,

$$\Psi(Z_\infty) \triangleq \lim_{m \rightarrow \infty} \frac{2(1 - \alpha)}{\alpha} [1 - (1 - \alpha)^m] = \frac{2(1 - \alpha)}{\alpha}$$

For  $Z$  computed by Eq. (11), we have

$$\psi(Z) \leq \frac{1}{s} \sum_i^s \Psi(Z_{m_i}) \triangleq \Psi(Z). \quad (28)$$

The proof of Lemma 5.3, detailed in Appendix A.5, progressively establishes bounds for  $\tilde{A}^m$ ,  $R_m$ ,  $Z_m$ , and  $Z$ . As defined in Definition 5.2, bounding the sensitivity involves constraining the row-wise differences  $\|z'_i - z_i\|_2$  (corresponding to bounding the sum of each row) and subsequently aggregating these differences across all rows  $i = 1, 2, \dots, n$  (corresponding to bounding the sum of each column). In terms of rows, we observe that the sum of each row in  $\tilde{A}^m$  and  $R_m$  consistently equals 1, a consequence of the normalization process ( $\tilde{A} = D^{-1}(A + I)$ ) and linear combination operations described in Section 4.3.2. However, bounding the columns of  $\tilde{A}^m$  and  $R_m$  is rather complex due to the intricacies introduced during propagation. To address this difficulty, we introduce Lemma 5.4, which serves as a cornerstone in the proof of Lemma 5.3. The proof



of Lemma 5.4 is detailed in Appendix A.6. Lemma 5.4 establishes that the sum of the  $j$ -th column of  $\tilde{A}^m$  or  $R_m$  is intrinsically linked to the degree of node  $j$ , irrespective of the number of propagation steps  $m$ . Remarkably, this relationship holds even when  $\tilde{A}^m$  undergoes an element-wise clipping, a technique frequently employed in DP algorithms. The implications of Lemma 5.4 extend beyond our analysis, offering valuable insights that can benefit future research in the realm of differentially private algorithms, especially in contexts where artificial clippings are commonplace.

LEMMA 5.4. *Let the elements in  $\tilde{A}$  satisfy the following constraints*

$$\tilde{A}_{ij} = \begin{cases} 0 & i \neq j \text{ \& } A_{ij} = 0 \\ \min(\frac{1}{k_i+1}, p) & i \neq j \text{ \& } A_{ij} = 1 \\ 1 - \sum_{u \neq i} \tilde{A}_{iu} & i = j \end{cases}$$

where  $k_i$  is the degree of node  $i$  and  $p \leq \frac{1}{2}$  is a bound on the off-diagonal elements in  $\tilde{A}$ . Especially, when  $p = \frac{1}{2}$ , it is equivalent to the original normalization (in Section 4.3.2) for  $\tilde{A}$  without any additional bound  $p$ . Then for any integer  $m \geq 1$ , we have

- Every entry of  $\tilde{A}^m$ ,  $R_m$ , or  $R_\infty$  is non-negative.
- The sum of each row of  $\tilde{A}^m$ ,  $R_m$ , or  $R_\infty$  is 1.
- The sum of column  $i$  of  $\tilde{A}^m$ ,  $R_m$ , or  $R_\infty$  is  $\leq \max((k_i+1)p, 1)$ .

### 5.3 Proof of Theorem 5.1

We are now ready to prove our main result, Theorem 5.1.

**Proof:** First, we bound the ratio  $\frac{g(\Theta_{priv}|G)}{g(\Theta_{priv}|G')}$  of the densities of  $\Theta_{priv}$  (from Eq. (17)) for neighboring graphs  $G$  and  $G'$ .

Let  $B = (b_1, b_2, \dots, b_c)$  and  $B' = (b'_1, b'_2, \dots, b'_c)$  denote the noise matrices sampled by the training algorithm on  $G$  and  $G'$  respectively. Let  $\Theta_{priv}$  be the optimal solution on both  $L_{priv}(\Theta; Z, Y)$  and  $L_{priv}(\Theta; Z', Y)$ , where  $Z$  and  $Z'$  are computed on  $G$  and  $G'$ , respectively. As  $\Theta_{priv}$  is optimal, the derivatives of the two loss functions are both 0 at  $\Theta = \Theta_{priv}$ ; accordingly, we have:

$$\begin{aligned} B &= -n_1 \frac{\partial (L_\Lambda(\Theta_{priv}; Z, Y) + \frac{1}{2} \Lambda' \|\Theta_{priv}\|_F^2)}{\partial \Theta_{priv}}, \\ B' &= -n_1 \frac{\partial (L_\Lambda(\Theta_{priv}; Z', Y) + \frac{1}{2} \Lambda' \|\Theta_{priv}\|_F^2)}{\partial \Theta_{priv}}. \end{aligned} \quad (29)$$

By Lemma A.3 that the mappings from  $\Theta_{priv}$  to  $B$  and  $B'$  in Eq. (29) are continuously differentiable and bijective, we can use Eq. (20.20) in [6] that the PDF of  $\Theta_{priv}$  on graphs  $G$  and  $G'$  can be expressed as

$$\frac{g(\Theta_{priv}|G)}{g(\Theta_{priv}|G')} = \frac{|\det(J(\Theta_{priv} \mapsto B|G))|^{-1}}{|\det(J(\Theta_{priv} \mapsto B'|G'))|^{-1}} \cdot \frac{\mu(B|G)}{\mu(B'|G')}, \quad (30)$$

where  $J(\Theta_{priv} \mapsto B|G)$  and  $J(\Theta_{priv} \mapsto B'|G')$  are the Jacobian matrices of the mappings from  $\Theta_{priv}$  to  $B$  and  $B'$  respectively, and  $\mu(\cdot)$  are the probability density functions. We separately bound the two ratios in the RHS and divide the privacy budget  $\epsilon$  into two parts  $\epsilon = \omega\epsilon + (1-\omega)\epsilon$  where  $\omega$  is a hyperparameter.

Let  $\Theta_{priv} = (\theta_1, \theta_2, \dots, \theta_c)$  where  $\theta_j \in \mathbb{R}^d$ ,  $j \in [1, c]$ . Observe from Eq. (12) that the derivatives of  $\ell(\Theta; z_i, \mathbf{y}_i)$  with respect to any of  $\theta_1, \theta_2, \dots, \theta_c$  are independent of each other. Therefore,  $J(\Theta_{priv} \mapsto B|G)$  and  $J(\Theta_{priv} \mapsto B'|G')$  are size  $dc \times dc$  block

diagonal matrices with size  $d \times d$  Jacobian matrices  $J(\theta_j \mapsto b_j|G)$  and  $J(\theta_j \mapsto b'_j|G')$ ,  $j \in [1, c]$ , lying on their diagonals, respectively. Let  $\ell'(x; y)$ ,  $\ell''(x; y)$ , and  $\ell'''(x; y)$  be the first, second, and third-order derivatives of  $\ell(x; y)$ . The specific forms of these derivatives are shown in Appendix A.4. According to Eq. (29),  $\theta_j \mapsto b_j|G$  and  $\theta_j \mapsto b'_j|G'$  are constructed by the following equations.

$$\begin{aligned} b_j &= - \sum_{i=1}^{n_1} z_i \ell'(z_i^T \theta_j; \mathbf{y}_{ij}) - n_1(\Lambda + \Lambda') \theta_j, \\ b'_j &= - \sum_{i=1}^{n_1} z'_i \ell'(z'_i{}^T \theta_j; \mathbf{y}_{ij}) - n_1(\Lambda + \Lambda') \theta_j, \end{aligned} \quad (31)$$

We can separately analyze the determinant of each of  $J(\theta_j \mapsto b_j|G)$  and  $J(\theta_j \mapsto b'_j|G')$ ,  $j \in [1, c]$  since

$$\frac{|\det(J(\Theta_{priv} \mapsto B|G))|^{-1}}{|\det(J(\Theta_{priv} \mapsto B'|G'))|^{-1}} = \prod_{j=1}^c \frac{|\det(J(\theta_j \mapsto b_j|G))|^{-1}}{|\det(J(\theta_j \mapsto b'_j|G'))|^{-1}} \quad (32)$$

For any  $\theta_j$ ,  $j \in [1, c]$ , there are two cases to consider: (i) for all  $j$ ,  $\|\theta_j\|_2 \leq c_\theta$  and (ii) there exists some  $j$  that  $\|\theta_j\|_2 > c_\theta$ .

**Case (i).** We consider the case (i) first. Lemma A.5 (presented in Appendix A.7) shows that for any  $\|\theta_j\|_2 \leq c_\theta$ ,  $j \in [1, c]$  we have

$$\frac{|\det(J(\theta_j \mapsto b_j|G))|^{-1}}{|\det(J(\theta_j \mapsto b'_j|G'))|^{-1}} \leq \left(1 + \frac{(2c_2 + c_3c_\theta)\Psi(Z)}{dn_1(\Lambda + \Lambda')}\right)^d.$$

Since  $\|\theta_j\|_2 \leq c_\theta$  for all  $j \in [1, c]$ , we have

$$\frac{|\det(J(\Theta_{priv} \mapsto B|G))|^{-1}}{|\det(J(\Theta_{priv} \mapsto B'|G'))|^{-1}} \leq \left(1 + \frac{(2c_2 + c_3c_\theta)\Psi(Z)}{dn_1(\Lambda + \Lambda')}\right)^{cd}.$$

As  $\Lambda' \geq 0$ , the above ratio of Jacobian matrices is bounded by  $\exp(\epsilon_\Lambda)$ , and the remaining budget for bounding  $\frac{\mu(B|G)}{\mu(B'|G')}$  is  $\exp(\epsilon - \epsilon_\Lambda)$ . We compress the above ratio to reserve more budget for the latter. So, we set a hyperparameter  $\omega$  to artificially bound the ratio by  $\exp(\epsilon - \omega\epsilon)$ . Then there are two cases to consider: (I)  $\epsilon_\Lambda \leq (1-\omega)\epsilon$ , which means that even if  $\Lambda' = 0$ , the remaining budget ( $\geq \omega\epsilon$ ) is sufficient, and (ii)  $\epsilon_\Lambda > (1-\omega)\epsilon$ , for which we set the additional parameter  $\Lambda'$  by Eq. (25). This ensures that the ratio can be bounded by  $\exp(\epsilon - \omega\epsilon)$ , with an exact budget of  $\omega\epsilon$  remaining. Therefore,

$$\frac{|\det(J(\Theta_{priv} \mapsto B|G))|^{-1}}{|\det(J(\Theta_{priv} \mapsto B'|G'))|^{-1}} \leq \exp(\min(\epsilon_\Lambda, \epsilon - \omega\epsilon)). \quad (33)$$

Lemma A.6 (in Appendix A.8) shows that for any  $\|\theta_j\|_2 \leq c_\theta$ ,  $j \in [1, c]$ , we have

$$\frac{\mu(b_j|G)}{\mu(b'_j|G')} \leq \exp(\beta(c_1 + c_2c_\theta)\Psi(Z)).$$

Since  $b_1, b_2, \dots, b_c$  are sampled independently and  $\|\theta_j\|_2 \leq c_\theta$  for all  $j \in [1, c]$  in the case (i), we have

$$\begin{aligned} \frac{\mu(B|G)}{\mu(B'|G')} &= \prod_j \frac{\mu(b_j|G)}{\mu(b'_j|G')} \\ &\leq \exp(c(c_1 + c_2c_\theta)\Psi(Z)\beta) \\ &\leq \exp(\max(\epsilon - \epsilon_\Lambda, \omega\epsilon)). \end{aligned} \quad (34)$$

where the last inequality substitutes  $\beta$  with Eq. (26).

In conclusion, combining with Eq. (30), (33), and (34), when  $\|\theta_j\|_2 \leq c_\theta$  for all  $j \in [1, c]$ , we have:

$$\begin{aligned} \frac{g(\Theta_{priv}|G)}{g(\Theta_{priv}|G')} &\leq \exp(\min(\epsilon_\Lambda, \epsilon - \omega\epsilon)) \exp(\max(\epsilon - \epsilon_\Lambda, \omega\epsilon)) \\ &= \exp(\epsilon). \end{aligned} \quad (35)$$

Similarly, we have  $\frac{g(\Theta_{priv}|G')}{g(\Theta_{priv}|G)} \leq \exp(\epsilon)$  when  $\|\theta_j\|_2 \leq c_\theta$  for all  $j \in [1, c]$ .

**Case (ii).** For the case (ii) that there exists some  $j$  that  $\|\theta_j\|_2 > c_\theta$ , we bound the probability that it happens by  $\delta$ . By the union bound,

$$\Pr[\cup_{j=1}^c \mathbb{1}(\|\theta_j\|_2 > c_\theta) = 1] \leq \sum_{j=1}^c \Pr[\|\theta_j\|_2 > c_\theta] \quad (36)$$

where  $\mathbb{1}$  is an indicator function.  $\mathbb{1}(\cdot) = 1$  denotes that the event  $\cdot$  happens and  $\mathbb{1}(\cdot) = 0$  otherwise. Since  $\|z_j\|_2 \leq 1$  and  $|l'| \leq c_1$ , when  $\|\theta_j\|_2 > c_\theta$ , by Eq. (31),

$$\|\mathbf{b}_j\|_2 \geq n_1(\Lambda + \Lambda')c_\theta - n_1c_1 \geq n_1(\Lambda c_\theta - c_1).$$

Hence,

$$\begin{aligned} \Pr[\|\theta_j\|_2 > c_\theta] &\leq \Pr[\|\mathbf{b}_j\|_2 > n_1(\Lambda c_\theta - c_1)] \\ &= \Pr[\|\mathbf{b}_j\|_2 > \frac{\beta n_1(\Lambda c_\theta - c_1)}{\beta}] \end{aligned} \quad (37)$$

Then we substitute  $\beta, c_\theta$  with Eq. (26) and (23),

$$\beta n_1(\Lambda c_\theta - c_1) = \frac{\max(\epsilon - \epsilon_\Lambda, \omega\epsilon)}{\omega\epsilon} c_{sf} \geq c_{sf}$$

Hence,

$$\Pr[\|\mathbf{b}_j\|_2 > n_1(\Lambda c_\theta - c_1)] \leq \Pr[\|\mathbf{b}_j\|_2 > \frac{c_{sf}}{\beta}] \quad (38)$$

Since the distribution of  $\|\mathbf{b}_j\|_2$  follows Eq. (16),

$$\begin{aligned} \Pr[\|\mathbf{b}_j\|_2 > \frac{c_{sf}}{\beta}] &= 1 - \int_0^{\frac{c_{sf}}{\beta}} \frac{x^{d-1} e^{-\beta x} \beta^d}{(d-1)!} dx \\ &= 1 - \int_0^{c_{sf}} \frac{x^{d-1} e^{-x}}{(d-1)!} dx \leq \frac{\delta}{c} \end{aligned} \quad (39)$$

where the last inequality substitutes  $c_{sf}$  with Eq. (20). Combining Eq. (36), (37), (38), and (39), we get

$$\Pr[\cup_{j=1}^c \mathbb{1}(\|\theta_j\|_2 > c_\theta) = 1] \leq \sum_{j=1}^c \frac{\delta}{c} = \delta \quad (40)$$

By Eq. (35) and (40), Algorithm 1 satisfies  $(\epsilon, \delta)$ -pDP (defined in Definition B.1 in Appendix B.1). By Lemma B.2, Algorithm 1 satisfies  $(\epsilon, \delta)$ -DP.

## 6 EXPERIMENTS

### 6.1 Experiment Settings

**6.1.1 Datasets.** Following previous work [24, 27, 28], we evaluate the methods on 4 real-world datasets with varied sizes and homophily ratios, as defined in Definition C.1 and ranging from 0 to 1. The homophily ratio indicates the tendency for vertices with identical labels to be connected. Specifically, we consider three homophily graphs (Cora-ML, CiteSeer, and PubMed) and one heterophily graph (Actor). Key statistics of these datasets are summarized in Table 1.

Following the convention [28], we use fixed training, validation, and testing sets for Cora-ML, CiteSeer, and PubMed. These include 20 samples per class in the training set, 500 samples in the validation set, and 1000 samples in the testing set. For Actor, we generate 5 random training/validation/testing splits with proportions of 60%/20%/20%, respectively, following [24]. The training and testing are conducted on the same graph and both require protection of edge privacy. For a fair comparison, we do not add noise during the inference phase of the baselines if they only use individual edges of the vertices (as explained in Section 4.3.6). We evaluate the methods' classification accuracy on the datasets by the micro-averaged F1 score (Micro F1), a metric that combines the precision and recall scores of the model.

**6.1.2 Competitors. GCN (Non-DP).** For the non-private baseline, we examine the traditional GCN [26] described in Section 2.1 on Cora-ML, CiteSeer, and PubMed, following [28]. On Actor, we examine GPR-GNN [9], following [24, 30]. GPR-GNN integrates aggregate features from various steps, serving a function similar to Eq. (11). The difference is that GPR-GNN assigns trainable coefficients before integrating the aggregation features, which can adaptively control the contribution of each propagation step. For simplicity, the two methods are collectively referred to as GCN (non-DP).

**DPGCN** [46]. DPGCN builds upon non-private GCNs by injecting noise into the adjacency matrix and replacing the original adjacency matrix with the noisy one.

**LPGNet** [28]. In LPGNet, the edges of each vertex are transformed into an embedding vector representing the statistics of classes (predicted by an MLP trained with vertex features) of its neighboring vertices. These embeddings are then concatenated with the original vertex features. The method iteratively refines the embeddings and predicts node classes through training MLPs.

**GAP** [40]. The GAP algorithm iteratively aggregates features by the adjacency matrix and adds noise to the aggregation results. It then concatenates the noisy aggregations and feeds the concatenation into the classification network.

**ProGAP** [39]. ProGAP, akin to its predecessor GAP, performs iterative feature aggregation using the adjacency matrix and adds noise to the aggregation results. Unlike GAP, ProGAP handles the aggregate features as follows: in each iteration, these features, once perturbed, are input into an additional MLP, whose output is then concatenated with the outputs from previous iterations. Finally, ProGAP feeds the concatenation into the classification network.

Note that LPGNet, GAP, and ProGAP all train an MLP to reduce feature dimension, without leveraging the edge information, an approach that fulfills a similar function to our feature encoder.

**MLP.** MLP denotes a simple MLP model that does not use graph edges and, thus, inherently satisfies edge DP for any privacy budget.

**6.1.3 Hyperparameters.** For the privacy constraints, we vary  $\epsilon$  across  $\{0.5, 1, 2, 3, 4\}$  and set  $\delta < \frac{1}{|E|}$  ( $|E|$  is the number of edges). When assessing the competitors, we follow their tuning strategies to report their best performance. Following the competitors [39, 40, 46], we do not account for the privacy loss incurred during hyperparameter tuning.

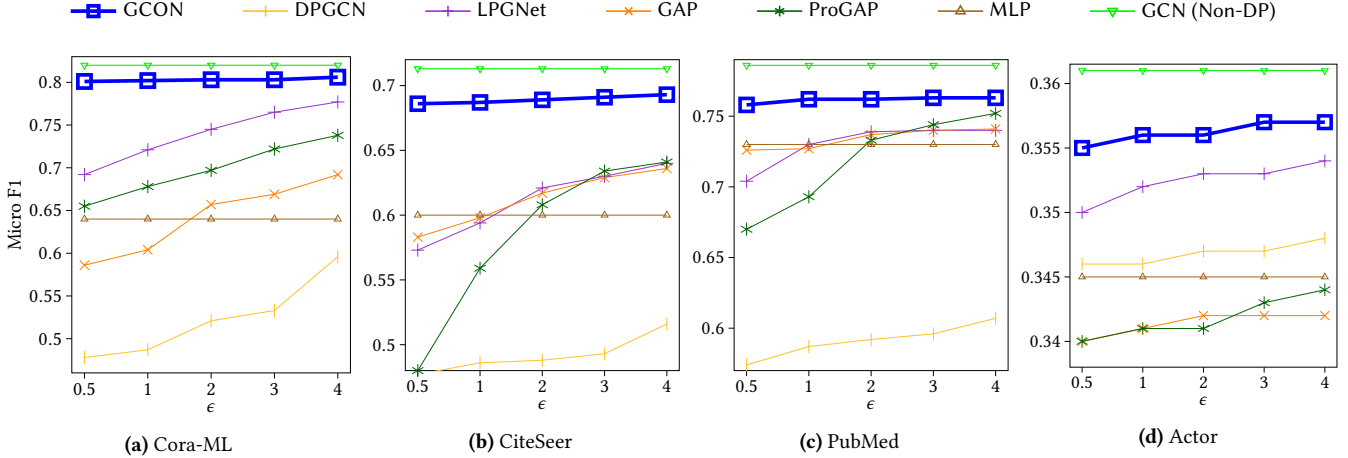


Figure 1: Algorithm Comparison: Micro F1 score.

## 6.2 Results

We repeat each experimental setup for 10 independent runs and report the average Micro F1 scores of the methods across varying  $\epsilon \in \{0.5, 1, 2, 3, 4\}$ . As depicted in Figure 1, GCON consistently outperforms the competitors in all configurations, indicating that the GCON model is not only more accurate but also demonstrates greater versatility across various privacy budgets and datasets.

Particularly, GCON achieves a higher performance improvement on homophily datasets Cora-ML, CiteSeer, and PubMed. In these datasets, vertices with identical labels are more likely to be connected. Recall from Sections 2.1 and 2.2 that both the standard GCN and the PPNP/APPNP propagation schemes aggregate neighbor vertices’ information through their edges, which are represented by the adjacency matrix ( $\tilde{A}$ ) or the propagation matrix. This aggregation (e.g.,  $\tilde{A}\mathbf{X}$ ) on homophily graphs facilitates the learning of node characteristics under each category, thereby improving classification accuracy. However, competing methods add noise directly to the adjacency matrix, disrupting their aggregation process and learning of classification due to interference from other categories. Thus, their performance deteriorates when the privacy budget  $\epsilon$  is small due to substantial injected noise, and improves as  $\epsilon$  increases. In contrast, GCON maintains an unaltered aggregation process and only introduces noise to  $\Theta \in \mathbb{R}^{d \times c}$  instead of overwhelming noise to  $\tilde{A} \in \mathbb{R}^{N \times N}$  or  $\tilde{A}\mathbf{X} \in \mathbb{R}^{N \times d}$  ( $N \gg c, d$ ). Therefore, GCON can withstand variations in privacy budget and maintain a superior performance close to the GCN (Non-DP) baseline. On the Actor dataset, the performance gap is smaller for different methods, since on this dataset, vertices with different labels are interconnected, and there is no clear pattern of vertices and their neighborhoods. This reduces the benefits of an unaltered neighbor aggregation; nonetheless, GCON outperforms all other DP competitors.

**Effect of the propagation steps  $m_1$ .** In what follows, we study the influence of the propagation step  $m_1$  in GCON on Cora-ML and CiteSeer with  $\epsilon = 4$ . We plot the performance under different  $\alpha \in \{0.2, 0.4, 0.6, 0.8\}$  in Figure 2.

First, compared with  $m_1 = 1$ , the performance with  $m_1 > 1$  is often larger, because a propagation matrix with larger  $m_1$  can

absorb richer information from a larger neighborhood, enabling the model to better understand the features of more vertices. However, when  $m_1$  increases to a certain extent, the performance of models with  $\alpha = 0.2$  and  $\alpha = 0.4$  decreases, due to the sensitivity and noise increase (as indicated in Lemma 5.3). As observed in Figure 2, setting  $m_1 \leq 10$  results in lower sensitivity and less additive noise compared to  $m_1 > 10$ , and ultimately, better performance. A similar phenomenon was also observed in the non-DP works [27], where they also claim the success of  $m_1 \leq 10$ . In conclusion, a propagation step of  $\leq 10$  is sufficient to achieve satisfactory results.

Furthermore, to remove the effect of private inference (described in Section 4.3.6) to better understand how our model’s performance varies with different choices of  $m_1$ , we also present the results and for GCON with non-private inference (namely, at the inference stage, all edge information are free to use without privacy constraints), referred to as GCON (NPI) in Appendix C.2. The results demonstrate that without privacy constraints at the inference stage, the positive impact of increasing  $m_1$  from 1 to 10 is much higher, which further justifies the usage of in our model.

**Effect of the restart probability  $\alpha$ .** In Figure 3, we report the accuracy of GCON on Cora-ML and CiteSeer with varying  $\alpha \in \{0.2, 0.4, 0.6, 0.8\}$  under  $\epsilon \in \{0.5, 1, 2, 3, 4\}$ , while  $m_1$  is tuned in a narrow range  $\{1, 2\}$ . For  $\alpha = 0.8$  and  $\alpha = 0.6$ , the model’s performance stabilizes at a higher level and gradually increases with  $\epsilon$ . However, for  $\alpha = 0.4$  and  $\alpha = 0.2$ , the performance is relatively poor when  $\epsilon = 0.5$  but rapidly increases to a level similar to that of  $\alpha = 0.8$  and  $\alpha = 0.6$  as  $\epsilon$  increases. The reason is that at lower  $\alpha$  values, the sensitivity  $\psi(Z_{m_1})$  (as indicated in Lemma 5.3) is relatively high, leading to a large amount of injected noise that hinders model performance. Moreover, even with an ample privacy budget ( $\epsilon = 3, 4$ ),  $\alpha = 0.2$  offers little improvement. Hence, a restart probability  $\alpha$  of  $\geq 0.4$  proves to be more broadly useful in practice.

Summarizing the experimental results, GCON outperforms its competitors in all settings, and, thus, is the method of choice in practical applications. Among the configurations of GCON, employing the APPR scheme with  $m \leq 10$  and a larger  $\alpha \geq 0.4$  is generally a good choice.

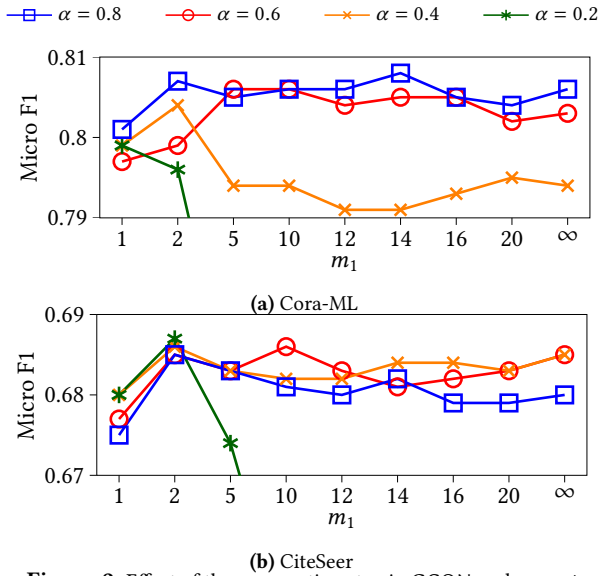


Figure 2: Effect of the propagation step in GCON under  $\epsilon = 4$ .

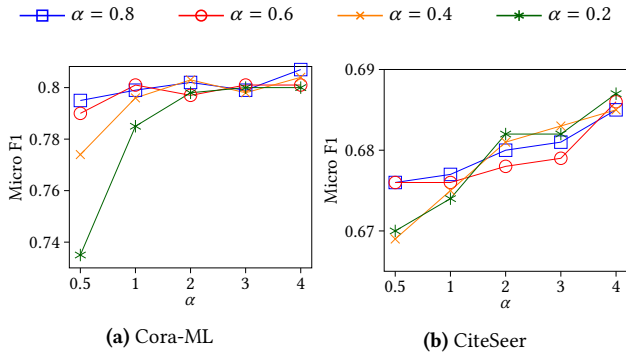


Figure 3: Effect of the restart probability  $\alpha$  in GCON.

## 7 RELATED WORK

Graph Neural Networks (GNNs) have emerged as a powerful tool for analyzing graph-structured data, which typically consists of nodes interconnected by complex edges representing relationships and dependencies. GNNs encompass various architectures, including Graph Convolutional Networks (GCNs), Graph Recurrent Neural Networks (GRNNs), and Graph Autoencoders (GAEs), with GCNs being particularly prevalent in node classification tasks due to their effectiveness and wide adoption in both research and practical applications [26, 48]. For a comprehensive overview of GNN variants and their applications, readers are referred to Wu et al. [48].

Privacy concerns also arise when using GNNs to analyze sensitive graph data, such as social networks and patient relationships [42]. There have been several successful privacy attacks. To briefly mention a few (non-exhaustive), Zhang et al. investigate privacy leakages in graph properties and propose several inference attacks [50]; Meng et al. present infiltration schemes for inferring neighboring links [32]; and He et al. develop a suite of black-box attacks targeting edge existence [21].

Differential Privacy (DP), whose application spans a variety of algorithms [14, 17], offers a rigorous framework for mitigating privacy risks in GNNs. DP is often achieved by injecting noise into

sensitive information. Here noise can be injected into various components of an algorithm, including its input [49], intermediate results [15], and the output [13]. Besides, objective function [7], which perturbs the objective function (of a strongly convex optimization problem) is also widely used in machine learning applications such as logistic regression. Training deep neural networks, on the other hand, often requires additional types of machinery such as privacy composition and data subsampling [2, 5, 33]. The aforementioned well-established techniques, however, do not automatically apply to training differentially private GCNs. The reason is that private data records (i.e., edges in the context of edge DP) in the sensitive input dataset of GCN training algorithms are usually correlated, as opposed to being independent as in other applications such as statistical machine learning, computer vision, and natural language processing [2, 7, 12, 37], etc.

Recent research on the combination of DP and GNNs primarily considers two DP definitions: edge DP and node DP. Edge DP prevents inferences about individual edges, while node DP protects all edges and the node itself [19, 25]. In this work, we focus on Edge-DP. Existing Edge-DP approaches in GNNs typically perturb the adjacency or aggregate feature matrix [28, 39, 40, 46]. For instance, DP-GCN [46] adds noise directly to the adjacency matrix, leading to significant distortions. GAP [40] uses the original adjacency matrix to aggregate node features first and then adds noise to the aggregate features. Building upon GAP, ProGAP [39] also employs an iterative process for feature aggregation using the adjacency matrix. The critical distinction lies in the handling of the perturbed aggregate features: in each iteration, these are processed through an MLP, and the resultant outputs across iterations are concatenated. LPGNet [28] breaks down graphs into independent nodes, and aggregates and then perturbs node features. Our work diverges from these methods by perturbing only the objective function, retaining the integrity of the graph convolutions, and enhancing classification accuracy. We also note that there is growing interest in GNNs with node DP [11] and decentralized graph data [29, 38], which is orthogonal to the focus of this work.

## 8 CONCLUSION

In this paper, we propose GCON, a novel algorithm for publishing GCNs with edge differential privacy. GCON is distinctive in its use of objective perturbation, which is challenging in the context of GCNs due to high sensitivity and non-convexity of traditional GCN architectures. The efficacy of GCON is primarily attributed to its unaltered graph convolution operations in the GCN. The privacy guarantee of GCON is rigorously established through formal proofs. We conducted a comprehensive series of experiments on popular graph datasets, exploring GCON’s performance under diverse privacy budget scenarios. The results from these experiments consistently demonstrate that it not only achieves significant improvements in accuracy over existing methods, but also exhibits robust generalization capabilities across various graphs.

Looking ahead, our future work aims to explore the development of additional propagation techniques to enhance model utility further. Additionally, we intend to expand the capabilities of GCON to handle tasks such as link prediction.

## REFERENCES

- [1] 2023. Apple Differential Privacy Technical Overview. (2023). Retrieved Aug 01, 2023 from [https://www.apple.com/privacy/docs/Differential\\_Privacy\\_Overview.pdf](https://www.apple.com/privacy/docs/Differential_Privacy_Overview.pdf)
- [2] Martin Abadi, Andy Chu, Ian Goodfellow, H Brendan McMahan, Ilya Mironov, Kunal Talwar, and Li Zhang. 2016. Deep learning with differential privacy. In *Proceedings of the 2016 ACM SIGSAC conference on computer and communications security*. 308–318.
- [3] Charu C Aggarwal. 2011. *An introduction to social network data analytics*. Springer.
- [4] Shun-ichi Amari. 1993. Backpropagation and stochastic gradient descent method. *Neurocomputing* 5, 4-5 (1993), 185–196.
- [5] Borja Balle and Yu-Xiang Wang. 2018. Improving the gaussian mechanism for differential privacy: Analytical calibration and optimal denoising. In *International Conference on Machine Learning*. PMLR, 394–403.
- [6] Patrick Billingsley. 2017. *Probability and measure*. John Wiley & Sons.
- [7] Kamalika Chaudhuri, Claire Monteleoni, and Anand D Sarwate. 2011. Differentially private empirical risk minimization. *Journal of Machine Learning Research* 12, 3 (2011).
- [8] Ming Chen, Zhewei Wei, Bolin Ding, Yaliang Li, Ye Yuan, Xiaoyong Du, and Ji-Rong Wen. 2020. Scalable graph neural networks via bidirectional propagation. *Advances in neural information processing systems* 33 (2020), 14556–14566.
- [9] Eli Chien, Jianhao Peng, Pan Li, and Olgica Milenkovic. 2020. Adaptive universal generalized pagerank graph neural network. *arXiv preprint arXiv:2006.07988* (2020).
- [10] Richard Courant and David Hilbert. 2008. *Methods of mathematical physics: partial differential equations*. John Wiley & Sons.
- [11] Ameya Daigavane, Gagan Madan, Aditya Sinha, Abhradeep Guha Thakurta, Gaurav Aggarwal, and Prateek Jain. 2021. Node-level differentially private graph neural networks. *arXiv preprint arXiv:2111.15521* (2021).
- [12] Soham De, Leonard Berrada, Jamie Hayes, Samuel L Smith, and Borja Balle. 2022. Unlocking high-accuracy differentially private image classification through scale. *arXiv preprint arXiv:2204.13650* (2022).
- [13] Cynthia Dwork. 2006. Differential privacy. In *International colloquium on automata, languages, and programming*. Springer, 1–12.
- [14] Cynthia Dwork, Aaron Roth, et al. 2014. The algorithmic foundations of differential privacy. *Foundations and Trends® in Theoretical Computer Science* 9, 3–4 (2014), 211–407.
- [15] Cynthia Dwork, Guy N Rothblum, and Salil Vadhan. 2010. Boosting and differential privacy. In *2010 IEEE 51st Annual Symposium on Foundations of Computer Science*. IEEE, 51–60.
- [16] Eric Goldman. 2020. An introduction to the california consumer privacy act (ccpa). *Santa Clara Univ. Legal Studies Research Paper* (2020).
- [17] Maoguo Gong, Yu Xie, Ke Pan, Kaiyuan Feng, and Alex Kai Qin. 2020. A survey on differentially private machine learning. *IEEE computational intelligence magazine* 15, 2 (2020), 49–64.
- [18] Brij Bhooshan Gupta, Akshat Gaurav, Enrique Caño Marín, and Wade Alhalabi. 2022. Novel graph-based machine learning technique to secure smart vehicles in intelligent transportation systems. *IEEE transactions on intelligent transportation systems* (2022).
- [19] Michael Hay, Chao Li, Jerome Miklau, and David Jensen. 2009. Accurate Estimation of the Degree Distribution of Private Networks. In *2009 Ninth IEEE International Conference on Data Mining*. 169–178. <https://doi.org/10.1109/ICDM.2009.11>
- [20] Xiangnan He, Kuan Deng, Xiang Wang, Yan Li, Yongdong Zhang, and Meng Wang. 2020. Lightgcn: Simplifying and powering graph convolution network for recommendation. In *Proceedings of the 43rd International ACM SIGIR conference on research and development in Information Retrieval*. 639–648.
- [21] Xinlei He, Jinyuan Jia, Michael Backes, Neil Zhenqiang Gong, and Yang Zhang. 2021. Stealing links from graph neural networks. In *30th USENIX Security Symposium (USENIX Security 21)*. 2669–2686.
- [22] Chris Jay Hoofnagle, Bart Van Der Sloot, and Frederik Zuiderveen Borgesius. 2019. The European Union general data protection regulation: what it is and what it means. *Information & Communications Technology Law* 28, 1 (2019), 65–98.
- [23] Roger A Horn and Charles R Johnson. 1991. *Topics in matrix analysis*, 1991. Cambridge University Press, Cambridge 37 (1991), 39.
- [24] Keke Huang, Wencai Cao, Hoang Ta, Xiaokui Xiao, and Pietro Liò. 2024. Optimizing Polynomial Graph Filters: A Novel Adaptive Krylov Subspace Approach. *arXiv preprint arXiv:2403.07954* (2024).
- [25] Shiva Prasad Kasiviswanathan, Kobbi Nissim, Sofya Raskhodnikova, and Adam Smith. 2013. Analyzing Graphs with Node Differential Privacy. In *Proceedings of the 10th Theory of Cryptography Conference on Theory of Cryptography (TCC’13)*. Springer-Verlag, Berlin, Heidelberg, 457–476. [https://doi.org/10.1007/978-3-642-36594-2\\_26](https://doi.org/10.1007/978-3-642-36594-2_26)
- [26] Thomas N Kipf and Max Welling. 2016. Semi-supervised classification with graph convolutional networks. *arXiv preprint arXiv:1609.02907* (2016).
- [27] Johannes Klicpera, Aleksandar Bojchevski, and Stephan Günnemann. 2019. Predict then Propagate: Graph Neural Networks meet Personalized PageRank. In *7th International Conference on Learning Representations, ICLR 2019, New Orleans, LA, USA, May 6-9, 2019*. OpenReview.net. <https://openreview.net/forum?id=H1gL-2A9Ym>
- [28] Aashish Kolluri, Teodora Baluta, Bryan Hooi, and Prateek Saxena. 2022. LPGNet: Link Private Graph Networks for Node Classification. In *Proceedings of the 2022 ACM SIGSAC Conference on Computer and Communications Security*. 1813–1827.
- [29] Wanyu Lin, Baochun Li, and Cong Wang. 2022. Towards private learning on decentralized graphs with local differential privacy. *IEEE Transactions on Information Forensics and Security* 17 (2022), 2936–2946.
- [30] Yao Ma, Xiaorui Liu, Neil Shah, and Jiliang Tang. 2021. Is homophily a necessity for graph neural networks? *arXiv preprint arXiv:2106.06134* (2021).
- [31] Kelong Mao, Jieming Zhu, Xi Xiao, Biao Lu, Zhaowei Wang, and Xiuqiang He. 2021. UltraGCN: ultra simplification of graph convolutional networks for recommendation. In *Proceedings of the 30th ACM International Conference on Information & Knowledge Management*. 1253–1262.
- [32] Lingshuo Meng, Yijie Bai, Yanjiao Chen, Yutong Hu, Wenyuan Xu, and Haiqin Weng. 2023. Devil in Disguise: Breaching Graph Neural Networks Privacy through Infiltration. In *Proceedings of the 2023 ACM SIGSAC Conference on Computer and Communications Security*. 1153–1167.
- [33] Ilya Mironov, Kunal Talwar, and Li Zhang. 2019. R\`enyi differential privacy of the sampled gaussian mechanism. *arXiv preprint arXiv:1908.10530* (2019).
- [34] Joe Near. 2018. Differential privacy at scale: Uber and berkeley collaboration. In *Enigma 2018 (Enigma 2018)*.
- [35] Lawrence Page, Sergey Brin, Rajeev Motwani, and Terry Winograd. 1999. *The PageRank citation ranking: Bringing order to the web*. Technical Report. Stanford InfoLab.
- [36] Adam Paszke, Sam Gross, Francisco Massa, Adam Lerer, James Bradbury, Gregory Chanan, Trevor Killeen, Zeming Lin, Natalia Gimelshein, Luca Antiga, et al. 2019. Pytorch: An imperative style, high-performance deep learning library. *Advances in neural information processing systems* 32 (2019).
- [37] Phillip Rust and Anders Søgaard. 2023. Differential privacy, linguistic fairness, and training data influence: Impossibility and possibility theorems for multilingual language models. In *International Conference on Machine Learning*. PMLR, 29354–29387.
- [38] Sina Sajadmanesh and Daniel Gatica-Perez. 2021. Locally private graph neural networks. In *Proceedings of the 2021 ACM SIGSAC conference on computer and communications security*. 2130–2145.
- [39] Sina Sajadmanesh and Daniel Gatica-Perez. 2023. ProGAP: Progressive Graph Neural Networks with Differential Privacy Guarantees. *arXiv preprint arXiv:2304.08928* (2023).
- [40] Sina Sajadmanesh, Ali Shahin Shamsabadi, Aurélien Bellet, and Daniel Gatica-Perez. 2023. Gap: Differentially private graph neural networks with aggregation perturbation. In *USENIX Security 2023-32nd USENIX Security Symposium*.
- [41] Jero Schäfer, Ming Tang, Danny Luu, Anke Katharina Bergmann, and Lena Wiese. 2022. Graph4Med: a web application and a graph database for visualizing and analyzing medical databases. *BMC bioinformatics* 23, 1 (2022), 537.
- [42] Jens Schrodt, Aleksei Dudchenko, Petra Knaup-Gregori, and Matthias Ganzinger. 2020. Graph-representation of patient data: a systematic literature review. *Journal of medical systems* 44, 4 (2020), 86.
- [43] Pauli Virtanen, Ralf Gommers, Travis E. Oliphant, Matt Haberland, Tyler Reddy, David Cournapeau, Evgeni Burovski, Pearu Peterson, Warren Weckesser, Jonathan Bright, Stéfan J. van der Walt, Matthew Brett, Joshua Wilson, K. Jarrod Millman, Nikolay Mayorov, Andrew R. J. Nelson, Eric Jones, Robert Kern, Eric Larson, C J Carey, Ilhan Polat, Yu Feng, Eric W. Moore, Jake VanderPlas, Denis Laxalde, Josef Perktold, Robert Cimman, Ian Henriksen, E. A. Quintero, Charles R. Harris, Anne M. Archibald, Antônio H. Ribeiro, Fabian Pedregosa, Paul van Mulbregt, and SciPy 1.0 Contributors. 2020. SciPy 1.0: Fundamental Algorithms for Scientific Computing in Python. *Nature Methods* 17 (2020), 261–272. <https://doi.org/10.1038/s41592-019-0686-2>
- [44] Jianian Wang, Sheng Zhang, Yanghua Xiao, and Rui Song. 2021. A review on graph neural network methods in financial applications. *arXiv preprint arXiv:2111.15367* (2021).
- [45] Jianxin Wei, Ergute Bao, Xiaokui Xiao, and Yin Yang. 2022. Dpis: An enhanced mechanism for differentially private sgd with importance sampling. In *Proceedings of the 2022 ACM SIGSAC Conference on Computer and Communications Security*. 2885–2899.
- [46] Fan Wu, Yunhui Long, Ce Zhang, and Bo Li. 2022. Linkteller: Recovering private edges from graph neural networks via influence analysis. In *2022 IEEE Symposium on Security and Privacy (SP)*. IEEE, 2005–2024.
- [47] Felix Wu, Amauri Souza, Tianyi Zhang, Christopher Fifty, Tao Yu, and Kilian Weinberger. 2019. Simplifying graph convolutional networks. In *International conference on machine learning*. PMLR, 6861–6871.
- [48] Zonghan Wu, Shirui Pan, Fengwen Chen, Guodong Long, Chengqi Zhang, and S Yu Philip. 2020. A comprehensive survey on graph neural networks. *IEEE transactions on neural networks and learning systems* 32, 1 (2020), 4–24.
- [49] Yuchen Yang, Haolin Yuan, Bo Hui, Neil Gong, Neil Fendley, Philippe Burlina, and Yinzi Cao. 2023. Fortifying Federated Learning against Membership Inference Attacks via Client-level Input Perturbation. In *2023 53rd Annual IEEE/IFIP International Conference on Dependable Systems and Networks (DSN)*. IEEE, 288–301.

- [50] Zhikun Zhang, Min Chen, Michael Backes, Yun Shen, and Yang Zhang. 2022. Inference attacks against graph neural networks. In *31st USENIX Security Symposium (USENIX Security 22)*. 4543–4560.
- [51] Jun Zhao, Teng Wang, Tao Bai, Kwok-Yan Lam, Zhiying Xu, Shuyu Shi, Xuebin Ren, Xinyu Yang, Yang Liu, and Han Yu. 2019. Reviewing and improving the Gaussian mechanism for differential privacy. *arXiv preprint arXiv:1911.12060* (2019).
- [52] Ying Zhao and Jinjun Chen. 2022. A survey on differential privacy for unstructured data content. *ACM Computing Surveys (CSUR)* 54, 10s (2022), 1–28.

## A MAIN THEORETICAL ARGUMENTS

### A.1 Lemma A.1 and its proof

In this section we prove matrix  $I - (1 - \alpha)\tilde{A}$  is invertible.

LEMMA A.1. *Matrix  $I - (1 - \alpha)\tilde{A}$  is invertible.*

**Proof:** The lemma holds iff the determinant  $\det(I - (1 - \alpha)\tilde{A}) \neq 0$ , i.e.,  $\det(\tilde{A} - \frac{1}{1-\alpha}I) \neq 0$ , which is the case iff  $\frac{1}{1-\alpha}$  is not an eigenvalue of  $\tilde{A}$  (by the fundamental theorem of algebra). Here we know that  $\frac{1}{1-\alpha}$  is always larger than 1 since  $\alpha \in (0, 1)$ . Next we prove that any eigenvalue  $\lambda$  of  $\tilde{A}$  satisfies  $|\lambda| \leq 1$ .

For any eigenvalue  $\lambda$  of  $\tilde{A}$ , let its corresponding eigenvector be  $x = (x_1, \dots, x_N)$ , i.e.,

$$\tilde{A}x = \lambda x.$$

Let  $i$  be the subscript such that  $|x_i| \geq |x_j|, \forall j \in [1, n]$  and let  $\tilde{a}_{ij}$  be the entry on the  $j$ -th column of the  $i$ -th row of matrix  $\tilde{A}$ . Focusing on the  $i$ -th dimension on both sides of the above equation, we have that

$$\sum_j^n \tilde{a}_{ij}x_j = \lambda x_i.$$

Taking the absolute values of both sides, we get

$$|\lambda x_i| = \left| \sum_j^n \tilde{a}_{ij}x_j \right| \leq \sum_j^n \tilde{a}_{ij}|x_j| \leq \sum_j^n \tilde{a}_{ij}|x_i| = |x_i|.$$

The first inequality follows from the fact that every element of  $\tilde{A}$  is non-negative (either 0 or 1) and the last equality follows since  $\sum_j^n \tilde{a}_{ij} = 1$  ( $\tilde{A} = D^{-1}\tilde{A}$  by definition). Hence,  $|\lambda| \leq 1 < \frac{1}{1-\alpha}$  and the proof follows.

### A.2 Lemmas related to $\mathcal{L}_\Lambda$

LEMMA A.2.  *$L(\Theta; z_i, \mathbf{y}_i)$  is convex w.r.t.  $\Theta$ .  $L_\Lambda(\Theta; Z, Y)$  is strongly convex w.r.t.  $\Theta$ .*

**Proof:** When  $y \in \{0, 1\}$ ,  $\ell''(x; y) > 0$ , so  $\ell(x; y)$  is convex. The Hessian matrix of  $\ell(z_i^T \theta_j; \mathbf{y}_{ij})$  w.r.t.  $\theta_j$  is  $z_i z_i^T \ell''(z_i^T \theta_j; \mathbf{y}_{ij})$ , whose eigenvalues is non-negative. Hence,  $\ell(z_i^T \theta_j; \mathbf{y}_{ij})$  is convex w.r.t.  $\theta_j$ .

The Hessian matrix of  $L(\Theta; z_i, \mathbf{y}_i)$  w.r.t.  $\Theta$  is a block matrix with  $z_i z_i^T \ell''(z_i^T \theta_j; \mathbf{y}_{ij}), j \in [1, c]$  locating on its diagonal and 0 on elsewhere. Hence, its eigenvalues is non-negative, i.e., it is convex w.r.t.  $\Theta$ . Then  $\sum_i^n L(\Theta; z_i, \mathbf{y}_i)$  is convex w.r.t.  $\Theta$ . Furthermore, since  $\frac{1}{2}\Lambda \|\Theta\|_F^2$  is strongly convex w.r.t.  $\Theta$ ,  $L_\Lambda(\Theta; Z, Y)$  is strongly convex w.r.t.  $\Theta$ .

LEMMA A.3. *Given fixed graph  $G$ , i.e., fixed  $Z$  and  $Y$ , for any noise  $B$ , the optimal solution  $\Theta_{priv}$  is unique. Moreover, the mapping from  $B$  (or  $B'$  on graph  $G'$ ) to  $\Theta_{priv}$  constructed by Eq. (29) is bijective and continuous differentiable w.r.t.  $\Theta_{priv}$ .*

**Proof:** As stated in Lemma A.2,  $L_\Lambda(\Theta_{priv}; Z, Y)$  is strongly convex w.r.t.  $\Theta$ . By Fact 1,  $L_\Lambda(\Theta_{priv}; Z, Y) + \frac{1}{2}\Lambda' \|\Theta\|_F^2$  is strongly convex. Hence, for a fixed  $B$ , the optimal solution  $\Theta_{priv}$  is unique and the mapping from  $B$  to  $\Theta_{priv}$  is injective.

Eq. (29) shows that for any  $\Theta_{priv}$ , there exists a  $B$  for which  $\Theta_{priv}$  is the minimizer so that the mapping from  $B$  to  $\Theta_{priv}$  is surjective.

In conclusion, for any graph  $G$ , i.e., fixed  $Z$  and  $Y$ , the mapping between  $\Theta_{priv}$  and  $B$  is bijective. As defined in Section 4.3.5,  $L_\Lambda$  has higher order and continuous derivatives. Hence, the mapping is continuous differentiable w.r.t.  $\Theta_{priv}$ . Similarly, the argument holds for  $B'$  on  $G'$ .

### A.3 Correctness of Algorithm 2

Here we prove the correctness of our sampling method (Algorithm 2).

LEMMA A.4. *Algorithm 2 uniformly samples a vector  $b$  on the  $d$ -dimensional hypersphere with radius  $a$ .*

**Proof:** We have vector  $\mathbf{u} = (u_1, u_2, \dots, u_d) \sim \mathcal{N}(0, I_d)$ . According to the rotational symmetry of the normal distribution, for any orthogonal matrix  $S$ , we can rotate  $\mathbf{u}$  to  $S\mathbf{u}$ , which is oriented in another direction and satisfies  $S\mathbf{u} \sim \mathcal{N}(0, I_d)$ , i.e.,  $\mathbf{u}$  and  $S\mathbf{u}$  follow the same distribution. Let  $\bar{\mathbf{u}} = a \frac{\mathbf{u}}{\|\mathbf{u}\|}$  and  $\bar{\mathbf{u}}_S = a \frac{S\mathbf{u}}{\|S\mathbf{u}\|} = a \frac{S\mathbf{u}}{\|\mathbf{u}\|}$ .  $\bar{\mathbf{u}}$  and  $\bar{\mathbf{u}}_S$  have the same length  $a$  and follow the same distribution for any rotation matrix  $S$ , i.e., each direction on the hypersphere with radius  $a$  is sampled with equal probability. Hence, the lemma is validated.

### A.4 Derivatives of $\ell(x; y)$

The following shows the first, second and third-order derivatives of  $\ell(x; y)$  (Eq. (13)), denoted as  $\ell'(x; y)$ ,  $\ell''(x; y)$ , and  $\ell'''(x; y)$ , respectively.

If  $\ell(x; y)$  is MultiLabel Soft Margin Loss,

$$\begin{aligned} \ell'(x; y) &= -\frac{1}{c} \left( y \frac{1}{1+e^x} + (1-y) \frac{-e^x}{1+e^x} \right) \\ \ell''(x; y) &= -\frac{1}{c} \left( y \frac{-e^x}{(1+e^x)^2} + (1-y) \frac{-e^x}{(1+e^x)^2} \right) \\ \ell'''(x; y) &= -\frac{1}{c} \left( y \frac{e^x(e^x-1)}{(1+e^x)^3} + (1-y) \frac{e^x(e^x-1)}{(1+e^x)^3} \right) \end{aligned}$$

The supremes of the absolute values of them are

$$\sup(|\ell'|) = \frac{1}{c}, \quad \sup(|\ell''|) = \frac{1}{4c}, \quad \sup(|\ell'''|) = \frac{1}{6\sqrt{3}c}$$

If  $\ell(x; y)$  is pseudo-Huber Loss,

$$\begin{aligned} \ell'(x; y) &= \frac{x-y}{c \sqrt{\frac{(x-y)^2}{\delta_l^2} + 1}} \\ \ell''(x; y) &= \frac{1}{c \cdot \left( \frac{(x-y)^2}{\delta_l^2} + 1 \right)^{\frac{3}{2}}} \\ \ell'''(x; y) &= -\frac{3(x-y)}{c \delta_l^2 \cdot \left( \frac{(x-y)^2}{\delta_l^2} + 1 \right)^{\frac{5}{2}}} \end{aligned}$$

The supremes of the absolute values of them are

$$\sup(|\ell'|) = \frac{\delta_l}{c}, \quad \sup(|\ell''|) = \frac{1}{c}, \quad \sup(|\ell'''|) = \frac{48\sqrt{5}}{125c\delta_l}$$

### A.5 Proof of Lemma 5.3

**Proof:** We prove Eqs. (27) & (28) sequentially.

**Proof for Eq. (27).** We prove Eq. (27) by examining the distinctions of  $\tilde{A}$ ,  $R_m$ , and  $Z_m$  on neighboring graphs one by one. Note that the computation of  $R_m$  and  $Z_m$  differs based on two propagation schemes: PPR ( $m = \infty$ ) and APPR ( $m \geq 0$ ). We begin with the case of PPR ( $m = \infty$ ).

Without loss of generality, we assume that  $G'$  is obtained from removing one edge between node 1 and node 2 in  $G$ . Let  $k_i$  be the degree of node  $i$  in  $G$ . We compute  $\tilde{A}$ ,  $R_\infty$ , and  $Z_\infty$  on  $G$  and  $\tilde{A}'$ ,  $R'_\infty$ , and  $Z'_\infty$  on  $G'$ . according to Section 4.3.2. When removing the edge, by definition, only the first and second rows in  $\tilde{A}$  change. In particular, both  $\tilde{A}_{12}$  and  $\tilde{A}_{21}$  change from  $\frac{1}{k_1+1}$  and  $\frac{1}{k_2+1}$  to 0.  $\tilde{A}_{11}$  and the entries of  $k_1 - 1$  neighbors of node 1 change from  $\frac{1}{k_1+1}$  to  $\frac{1}{k_1}$  respectively. It is similar for  $\tilde{A}_{22}$  and the  $k_2 - 1$  neighbors of node 2. Hence, we have

$$\Delta\tilde{A} \triangleq \tilde{A}' - \tilde{A} = \mathbf{v}_1 \mathbf{a}_1^T + \mathbf{v}_2 \mathbf{a}_2^T. \quad (41)$$

Here  $\mathbf{v}_1 = (1, 0, \dots, 0)^T$  and  $\mathbf{v}_2 = (0, 1, 0, \dots, 0)^T$ .  $\mathbf{a}_1 \in \mathbb{R}^n$  is a vector whose second entry is  $-\frac{1}{k_1+1}$ ,  $k_1$  entries are  $\frac{1}{k_1(k_1+1)}$ , and others are 0.  $\mathbf{a}_2$  is similar. Then,

$$\begin{aligned} \Delta R_\infty &\triangleq R'_\infty - R_\infty = R'_\infty R_\infty^{-1} R_\infty - R'_\infty R_\infty^{-1} R_\infty \\ &= \frac{1-\alpha}{\alpha} R'_\infty \Delta\tilde{A} R_\infty, \end{aligned} \quad (42)$$

$$\begin{aligned} \Delta Z_\infty &\triangleq Z'_\infty - Z_\infty = \Delta R_\infty X \\ &= \frac{1-\alpha}{\alpha} R'_\infty \Delta\tilde{A} R_\infty X \\ &= \frac{1-\alpha}{\alpha} R'_\infty (\mathbf{v}_1 \mathbf{a}_1^T Z_\infty + \mathbf{v}_2 \mathbf{a}_2^T Z_\infty). \end{aligned} \quad (43)$$

By Lemma 5.4 with  $p = \frac{1}{2}$ , the sum of column  $i$  of  $R'_\infty$  is at most  $\max(\frac{k'_i+1}{2}, 1)$ , where  $k'_i$  is the degree of node  $i$  in  $G'$ . Since  $G'$  is obtained from  $G$  by removing one edge between nodes 1 and 2, we have  $k_1 \geq 1$  and  $k_2 \geq 1$ . Hence, we have that

$$\|R'_\infty \mathbf{v}_1\|_1 \leq \frac{k_1+1}{2}, \quad \|R'_\infty \mathbf{v}_2\|_1 \leq \frac{k_2+1}{2}. \quad (44)$$

Let  $\mathbf{x}_i$ ,  $\mathbf{r}_{\infty,i}$  and  $\mathbf{z}_{\infty,i}$  denote the  $i$ -th rows of  $X$ ,  $R_\infty$  and  $Z_\infty$ , respectively. Assume that  $\|\mathbf{x}_i\|_2 \leq 1$ . By Lemma 5.4, the sum of each row of  $R_\infty$  is 1, for all  $i \in [1, n]$ , we have

$$\|\mathbf{z}_{\infty,i}\|_2 = \|\mathbf{r}_{\infty,i}^T X\|_2 = \|\mathbf{r}_{\infty,i}^T\|_1 \max_i \|\mathbf{x}_i\|_2 \leq 1.$$

Then we have that

$$\|\mathbf{a}_1^T Z_\infty\|_2 \leq \frac{2}{k_1+1}, \quad \|\mathbf{a}_2^T Z_\infty\|_2 \leq \frac{2}{k_2+1} \quad (45)$$

Using Eqs. (44) & (45),

$$\begin{aligned} \psi(Z_\infty) &\leq \|R'_\infty \mathbf{v}_1\|_1 \|\mathbf{a}_1^T Z_\infty\|_2 + \|R'_\infty \mathbf{v}_2\|_1 \|\mathbf{a}_2^T Z_\infty\|_2 \\ &\leq \frac{2(1-\alpha)}{\alpha} \triangleq \Psi(Z_\infty). \end{aligned} \quad (46)$$

Eq. (46) quantifies the changes in the  $\mathcal{L}_2$  norms of rows in  $Z_\infty$  when modifying one edge in the PPR scheme.

Next, we consider the other case of APPR ( $m \geq 0$ ). For  $m = 0$ , we have

$$\psi(Z_0) = \psi(IX) = 0 = \frac{2(1-\alpha)}{\alpha} [1 - (1-\alpha)^0].$$

For any  $m \geq 1$ , we define

$$\Delta\tilde{A}^m \triangleq \tilde{A}'^m - \tilde{A}^m.$$

We have

$$R'_m - R_m = \alpha \sum_{i=1}^{m-1} (1-\alpha)^i \Delta\tilde{A}^i + (1-\alpha)^m \Delta\tilde{A}^m. \quad (47)$$

By triangle inequality,

$$\psi(Z_m) \leq \alpha \sum_{i=1}^{m-1} (1-\alpha)^i \psi(\tilde{A}^i X) + (1-\alpha)^m \psi(\tilde{A}^m X). \quad (48)$$

Hence, the key to calculate the bounds for  $\psi(Z_m)$  is calculating  $\psi(\tilde{A}^m X)$ . We have known that  $\Delta\tilde{A} = \mathbf{v}_1 \mathbf{a}_1^T + \mathbf{v}_2 \mathbf{a}_2^T$ . For any two matrices  $M_1$  and  $M_2$ , the matrix  $M_1 \mathbf{v}_1 \mathbf{a}_1^T M_2$  is still in the form of a column by a row, of which the sum of norm of rows can be bounded similarly as Eqs. (44) & (45). Therefore, the key to calculating  $\psi(\tilde{A}^m X)$  is splitting  $\Delta\tilde{A}^m$  into addition of  $M_1 \Delta\tilde{A} M_2$ , which is an addition of a column by a row. When  $m = 1$ ,

$$\psi(\tilde{A} X) \leq 2 \frac{2}{k_1+1} \leq 2.$$

When  $m \geq 2$ ,

$$\Delta\tilde{A}^m = \frac{1}{2} [\Delta\tilde{A}^{m-1} (\tilde{A}' + \tilde{A}) + (\tilde{A}'^{m-1} + \tilde{A}^{m-1}) \Delta\tilde{A}]. \quad (49)$$

As shown above, we can recursively decompose  $\Delta\tilde{A}^m$  to  $\Delta\tilde{A}^{m-1}$ ,  $\Delta\tilde{A}^{m-2}$ ,  $\dots$  and finally an addition of  $M_1 \Delta\tilde{A} M_2$ . Then following a similar derivation as Eqs. (44) & (45), we have

$$\psi(\tilde{A}^m X) \leq 2m. \quad (50)$$

Combining Eqs. (50) & (48),

$$\psi(Z_m) \leq \frac{2(1-\alpha)}{\alpha} [1 - (1-\alpha)^m] \triangleq \Psi(Z_m). \quad (51)$$

Hence, Eq. (27) holds for any  $m \in [0, \infty]$ .

**Proof for Eq. (28).** Let  $\mathbf{z}_i$  and  $\mathbf{z}_{m,i}$  denote the  $i$ -th rows of  $Z$  and  $Z_m$ , respectively. We have

$$\begin{aligned} \psi(Z) &= \sum_{i=1}^n \|\mathbf{z}'_i - \mathbf{z}_i\|_2 \leq \sum_{i=1}^n \frac{1}{s} \sum_{j=1}^s \|\mathbf{z}'_{m,j,i} - \mathbf{z}_{m,j,i}\|_2 \\ &= \frac{1}{s} \sum_{j=1}^s \psi(Z_{m_j}) \leq \frac{1}{s} \sum_{j=1}^s \Psi(Z_{m_j}), \end{aligned}$$

where the first inequality follows from the triangle inequality. Hence, Eq. (28) holds.

In summary, Lemma 5.3 holds.

## A.6 Proof of Lemma 5.4

**Proof:**

For the first conclusion, following our normalization, every entry of  $\tilde{A}$  is non-negative. Since  $\tilde{A}^m$ ,  $R_m$  and  $R_\infty$  are polynomials w.r.t.  $\tilde{A}$  with positive coefficients, every entry of them is non-negative.

For the second conclusion, by definition, the sum of each row of  $\tilde{A}$  is 1. Then the sum of each row of  $\tilde{A}^m$  is 1. Using the fact that the sum of each row of  $I$  is 1, for each row of  $R_m$ , its sum is

$$1 \cdot \alpha \sum_{j=0}^{m-1} (1-\alpha)^j + 1 \cdot (1-\alpha)^m = 1$$

The above equation holds for any  $m > 0$  including  $m \rightarrow \infty$ , i.e.,  $R_m \rightarrow R_\infty$ .

Next, we prove the third conclusion. Since every entry of  $\tilde{A}$  is non-negative, we get that every entry of  $\tilde{A}^m$  is non-negative. Let  $v_{m,i}$  be the  $i$ th column of  $\tilde{A}^m$ . Let  $N_i$  be the set of neighbors of  $i$  and let  $k_i = |N_i|$ . We show by induction on  $m$  for any  $m \geq 1$  that: for any  $i$ ,  $|v_{m,i}|_1 \leq \max((k_i+1)p, 1)$ . In our proof, we leverage that  $A$  is symmetric.

When  $m = 1$ ,  $\tilde{A}^m = \tilde{A}$ .

$$\begin{aligned} |v_{m,i}|_1 &= \sum_{j \in N_i} \min\left(\frac{1}{k_j+1}, p\right) + (1 - k_i \min\left(\frac{1}{k_i+1}, p\right)) \\ &\leq k_i p + \max\left(\frac{1}{k_i+1}, 1 - k_i p\right) \\ &= \max\left(\frac{1}{k_i+1} + k_i p, 1\right) \end{aligned}$$

(1) If  $\frac{1}{k_i+1} < p$ ,  $\max(\frac{1}{k_i+1} + k_i p, 1) \leq (k_i+1)p = \max((k_i+1)p, 1)$ .

(2) If  $\frac{1}{k_i+1} \geq p$ ,  $\max(\frac{1}{k_i+1} + k_i p, 1) \leq 1 = \max((k_i+1)p, 1)$ .

Hence, the lemma holds when  $m = 1$ .

When  $m > 1$  and  $|v_{m,i}|_1 \leq \max((k_i+1)p, 1)$ . As  $\tilde{A}^{m+1} = \tilde{A}^m \cdot \tilde{A}$ , we have

$$\begin{aligned} |v_{m+1,i}|_1 &= \sum_{j \in N_i} \min\left(\frac{1}{k_j+1}, p\right) |v_{m,j}|_1 + \\ &\quad (1 - k_i \min\left(\frac{1}{k_i+1}, p\right)) |v_{m,i}|_1 \\ &\leq p \sum_{j \in N_i} \min\left(\frac{1}{(k_j+1)p}, 1\right) \max((k_j+1)p, 1) + \\ &\quad (1 - k_i \min\left(\frac{1}{k_i+1}, p\right)) \max((k_i+1)p, 1) \\ &= k_i p + \max\left(\frac{1}{k_i+1}, 1 - k_i p\right) \max((k_i+1)p, 1). \end{aligned}$$

(1) If  $\frac{1}{k_i+1} < p$ ,

$$\begin{aligned} &k_i p + \max\left(\frac{1}{k_i+1}, 1 - k_i p\right) \max((k_i+1)p, 1) \\ &\leq k_i p + \frac{1}{k_i+1} \cdot (k_i+1)p \\ &= (k_i+1)p = \max((k_i+1)p, 1). \end{aligned}$$

(2) If  $\frac{1}{k_i+1} \geq p$ ,

$$\begin{aligned} &k_i p + \max\left(\frac{1}{k_i+1}, 1 - k_i p\right) \max((k_i+1)p, 1) \\ &\leq k_i p + (1 - k_i p) \cdot 1 \\ &= 1 = \max((k_i+1)p, 1). \end{aligned}$$

Hence,  $|v_{m+1,i}|_1 \leq \max((k_i+1)p, 1)$ , i.e., the lemma holds for any  $m \geq 1$ .

For  $R_m$ , by Eq. (6),

$$R_m = \alpha \sum_{i=0}^{m-1} (1-\alpha)^i \tilde{A}^i + (1-\alpha)^m \tilde{A}^m.$$

Using the above conclusion of  $\tilde{A}^m$ , the sum of column  $i$  of  $R_m$  satisfies

$$\begin{aligned} &\leq \left( \alpha \sum_{j=0}^{m-1} (1-\alpha)^j + (1-\alpha)^m \right) \cdot \max((k_i+1)p, 1) \\ &= \max((k_i+1)p, 1). \end{aligned}$$

The above inequality holds for  $R_m$  with any  $m$ , so it holds for  $m \rightarrow \infty$ , i.e.,  $R_m \rightarrow R_\infty$ .

In summary, we have the sum of column  $i$  of  $\tilde{A}^m$ ,  $R_m$ , or  $R_\infty$  is  $\leq \max((k_i+1)p, 1)$ .

## A.7 Proof of Lemma A.5

LEMMA A.5. *Following the setting in Theorem 5.1, for any  $j \in [1, c]$ , when  $\|\theta_j\| \leq c_\theta$ ,*

$$\frac{|\det(J(\theta_j \mapsto \mathbf{b}_j|G))|^{-1}}{|\det(J(\theta_j \mapsto \mathbf{b}'_j|G'))|^{-1}} \leq \left(1 + \frac{(2c_2 + c_3 c_\theta) \Psi_Z(R_m)}{dn_1(\Lambda + \Lambda')}\right)^d \quad (52)$$

**Proof:**

Without loss of generality, we first establish the bound for  $\theta_1$ . Define

$$\mathbf{B}_1 \triangleq \sum_{i=1}^{n_1} \mathbf{z}_i \mathbf{z}_i^T \ell''(\mathbf{z}_i^T \theta_1; \mathbf{y}_{i1}) + n_1(\Lambda + \Lambda') \mathbf{I}_d, \quad (53)$$

$$\mathbf{E}_1 \triangleq - \sum_{i=1}^{n_1} \mathbf{z}_i \mathbf{z}_i^T \ell''(\mathbf{z}_i^T \theta_1; \mathbf{y}_{i1}) + \sum_{i=1}^{n_1} \mathbf{z}'_i \mathbf{z}'_i{}^T \ell''(\mathbf{z}'_i{}^T \theta_1; \mathbf{y}_{i1}), \quad (54)$$

where  $\mathbf{I}_d \in \mathbb{R}^{d \times d}$  is an identity matrix. Then  $\mathbf{J}(\theta_1 \mapsto \mathbf{b}_1|G) = -\mathbf{B}_1$  and  $\mathbf{J}(\theta_1 \mapsto \mathbf{b}'_1|G') = -(\mathbf{B}_1 + \mathbf{E}_1)$ . Let  $\sigma_i(\cdot)$  denote the  $i$ -th singular value of matrix  $\cdot$ , ordered non-increasingly, i.e.,  $\sigma_1 \geq \sigma_2 \geq \dots$ . We



have

$$\begin{aligned}
\frac{|\det(J(\boldsymbol{\theta}_1 \mapsto \mathbf{b}_1|G))^{-1}|}{|\det(J(\boldsymbol{\theta}_1 \mapsto \mathbf{b}'_1|G'))^{-1}|} &= \frac{|\det(\mathbf{B}_1 + \mathbf{E}_1)|}{|\det(\mathbf{B}_1)|} \\
&= |\det(\mathbf{B}_1^{-1}) \det(\mathbf{B}_1 + \mathbf{E}_1)| \\
&= |\det(I + \mathbf{B}_1^{-1} \mathbf{E}_1)| \\
&= \prod_i^d \sigma_i(I + \mathbf{B}_1^{-1} \mathbf{E}_1) \\
&\leq \prod_i^d (1 + \sigma_i(\mathbf{B}_1^{-1} \mathbf{E}_1)) \\
&\leq \left(1 + \frac{1}{d} \sum_i^d \sigma_i(\mathbf{B}_1^{-1} \mathbf{E}_1)\right)^d \quad (55) \\
&\leq \left(1 + \frac{1}{d} \sum_i^d \sigma_1(\mathbf{B}_1^{-1}) \sigma_i(\mathbf{E}_1)\right)^d \quad (56)
\end{aligned}$$

where the inequality 55 uses the GM-AM inequality (geometric mean  $\leq$  arithmetic mean), the inequality 56 uses Lemma B.4. Since  $\mathbf{B}_1$ ,  $\mathbf{E}_1$ , and  $\mathbf{B}_1^{-1}$  are Hermite matrices, their ordered singular values equal their absolute eigenvalues, i.e.,  $\sigma_i = |\lambda_i|, \forall i \in [1, d]$ . Observe the definition equation of  $\mathbf{B}_1$  that  $\lambda_i(\mathbf{B}_1) \geq n_1(\Lambda + \Lambda'), \forall i \in [1, d]$ . Equivalently,  $\forall i \in [1, d]$ ,

$$\sigma_i(\mathbf{B}_1^{-1}) = \lambda_i(\mathbf{B}_1^{-1}) \leq \frac{1}{n_1(\Lambda + \Lambda')}. \quad (57)$$

Next we analyze  $\sigma_i(\mathbf{E}_1)$ . We split  $\mathbf{E}_1 = \mathbf{E}_1^{(1)} + \mathbf{E}_1^{(2)}$  into two terms where

$$\begin{aligned}
\mathbf{E}_1^{(1)} &\triangleq \sum_{i=1}^{n_1} (\mathbf{z}'_i \mathbf{z}'_i{}^T - \mathbf{z}_i \mathbf{z}_i{}^T) \ell''(\mathbf{z}'_i{}^T \boldsymbol{\theta}_1; \mathbf{y}_{i1}), \\
\mathbf{E}_1^{(2)} &\triangleq \sum_{i=1}^{n_1} \mathbf{z}'_i \mathbf{z}'_i{}^T [\ell''(\mathbf{z}'_i{}^T \boldsymbol{\theta}_1; \mathbf{y}_{i1}) - \ell''(\mathbf{z}_i{}^T \boldsymbol{\theta}_1; \mathbf{y}_{i1})].
\end{aligned} \quad (58)$$

For  $\mathbf{E}_1^{(1)}$ , we have

$$\mathbf{E}_1^{(1)} = \sum_{i=1}^{n_1} [(\mathbf{z}'_i - \mathbf{z}_i) \mathbf{z}'_i{}^T \ell''(\mathbf{z}'_i{}^T \boldsymbol{\theta}_1; \mathbf{y}_{i1}) + \mathbf{z}_i (\mathbf{z}'_i{}^T - \mathbf{z}_i{}^T) \ell''(\mathbf{z}'_i{}^T \boldsymbol{\theta}_1; \mathbf{y}_{i1})]$$

Observe that the rank of  $(\mathbf{z}'_i - \mathbf{z}_i) \mathbf{z}'_i{}^T \ell''(\mathbf{z}'_i{}^T \boldsymbol{\theta}_1; \mathbf{y}_{i1})$  is 1 and its single non-zero singular value is

$$\begin{aligned}
\sigma &= \max_{\|\mathbf{x}\|_2=1} \|(\mathbf{z}'_i - \mathbf{z}_i) \mathbf{z}'_i{}^T \ell''(\mathbf{z}'_i{}^T \boldsymbol{\theta}_1; \mathbf{y}_{i1}) \mathbf{x}\|_2 \\
&= |\ell''(\mathbf{z}'_i{}^T \boldsymbol{\theta}_1; \mathbf{y}_{i1})| \max_{\|\mathbf{x}\|_2=1} \sqrt{\mathbf{x}^T \mathbf{z}'_i (\mathbf{z}'_i - \mathbf{z}_i)^T \cdot (\mathbf{z}'_i - \mathbf{z}_i) \mathbf{z}'_i{}^T \mathbf{x}} \\
&= |\ell''(\mathbf{z}'_i{}^T \boldsymbol{\theta}_1; \mathbf{y}_{i1})| \|\mathbf{z}'_i - \mathbf{z}_i\|_2 \|\mathbf{z}'_i\|_2 \\
&\leq c_2 \|\mathbf{z}'_i - \mathbf{z}_i\|_2
\end{aligned}$$

Similarly,  $\mathbf{z}_i (\mathbf{z}'_i{}^T - \mathbf{z}_i{}^T) \ell''(\mathbf{z}'_i{}^T \boldsymbol{\theta}_1; \mathbf{y}_{i1})$  has only one non-zero singular value that can be bounded by  $c_2 \|\mathbf{z}'_i - \mathbf{z}_i\|_2$ . According to Theorem B.3, the sum of singular values of  $\mathbf{E}_1^{(1)}$  can be bounded by

$$\sum_j^d \sigma_j(\mathbf{E}_1^{(1)}) \leq \sum_i^{n_1} 2c_2 \|\mathbf{z}'_i - \mathbf{z}_i\|_2 \leq 2c_2 \Psi(\mathbf{Z}) \quad (59)$$

For  $\mathbf{E}_1^{(2)}$ , we rewrite it as  $\mathbf{E}_1^{(2)} = \sum_{i=1}^{n_1} \mathbf{E}_{1,i}^{(2)}$  where

$$\mathbf{E}_{1,i}^{(2)} \triangleq \mathbf{z}'_i \mathbf{z}'_i{}^T [\ell''(\mathbf{z}'_i{}^T \boldsymbol{\theta}_1; \mathbf{y}_{i1}) - \ell''(\mathbf{z}_i{}^T \boldsymbol{\theta}_1; \mathbf{y}_{i1})].$$

observe that  $\mathbf{z}'_i \mathbf{z}'_i{}^T$  is of rank 1 and  $\ell''$  is a scalar, so  $\mathbf{E}_{1,i}^{(2)}$  has rank  $\leq 1$ .  $\ell''$  is Lipschitz continuous and let  $c_3$  be its Lipschitz constant. When  $\|\boldsymbol{\theta}_1\|_2 \leq c_\theta$  where  $c_\theta$  is a constant introduced later in Eq. (23), we can bound the single non-zero singular value of  $\mathbf{E}_{1,i}^{(2)}$  by

$$\begin{aligned}
\sigma(\mathbf{E}_{1,i}^{(2)}) &= |\ell''(\mathbf{z}'_i{}^T \boldsymbol{\theta}_1; \mathbf{y}_{i1}) - \ell''(\mathbf{z}_i{}^T \boldsymbol{\theta}_1; \mathbf{y}_{i1})| \|\mathbf{z}'_i{}^T\|_2 \|\mathbf{z}'_i\|_2 \\
&\leq |\ell''(\mathbf{z}'_i{}^T \boldsymbol{\theta}_1; \mathbf{y}_{i1}) - \ell''(\mathbf{z}_i{}^T \boldsymbol{\theta}_1; \mathbf{y}_{i1})| \\
&\leq c_3 \|\boldsymbol{\theta}_1\|_2 \|\mathbf{z}'_i - \mathbf{z}_i\|_2 \\
&\leq c_3 c_\theta \|\mathbf{z}'_i - \mathbf{z}_i\|_2.
\end{aligned}$$

Hence,

$$\sum_i^d \sigma_i(\mathbf{E}_1^{(2)}) \leq \sum_i^{n_1} c_3 c_\theta \|\mathbf{z}'_i - \mathbf{z}_i\|_2 \leq c_3 c_\theta \Psi(\mathbf{Z}), \quad (60)$$

where the first inequality applies Theorem B.3. Combining Eq. (59) & (60), we get

$$\begin{aligned}
\sum_i^d \sigma_i(\mathbf{E}_1) &\leq \sum_j^d \sigma_j(\mathbf{E}_1^{(1)}) + \sum_i^d \sigma_i(\mathbf{E}_1^{(2)}) \\
&\leq (2c_2 + c_3 c_\theta) \Psi(\mathbf{Z}),
\end{aligned} \quad (61)$$

where the first inequality applies Corollary 3.4.3 in [23].

Combining Eq. (56), (57), & (61)

$$\frac{|\det(J(\boldsymbol{\theta}_1 \mapsto \mathbf{b}_1|G))^{-1}|}{|\det(J(\boldsymbol{\theta}_1 \mapsto \mathbf{b}'_1|G'))^{-1}|} \leq \left(1 + \frac{(2c_2 + c_3 c_\theta) \Psi(\mathbf{Z})}{dn_1(\Lambda + \Lambda')}\right)^d \quad (62)$$

The upper bound shown above also applies to any other

$$\frac{|\det(J(\boldsymbol{\theta}_j \mapsto \mathbf{b}_j|G))^{-1}|}{|\det(J(\boldsymbol{\theta}_j \mapsto \mathbf{b}'_j|G'))^{-1}|}, j \in [1, c].$$

## A.8 Proof of Lemma A.6

LEMMA A.6. *Following the setting in Theorem 5.1, for any  $j \in [1, c]$ , when  $\|\boldsymbol{\theta}_j\| \leq c_\theta$ ,*

$$\frac{\mu(\mathbf{b}_j|G)}{\mu(\mathbf{b}'_j|G')} \leq \exp(\beta(c_1 + c_2 c_\theta) \Psi_Z(\mathbf{R}_m)) \quad (63)$$

**Proof:** According to Eq. (31), for any  $j \in [1, C]$ ,

$$\begin{aligned}
\|\mathbf{b}'_j - \mathbf{b}_j\|_2 &= \left\| \sum_{i=1}^{n_1} \left( \mathbf{z}'_i \ell'(\mathbf{z}'_i{}^T \boldsymbol{\theta}_j; \mathbf{y}_{ij}) - \mathbf{z}_i \ell'(\mathbf{z}_i{}^T \boldsymbol{\theta}_j; \mathbf{y}_{ij}) \right) \right\|_2 \\
&= \left\| \sum_{i=1}^{n_1} \left( \mathbf{z}'_i (\ell'(\mathbf{z}'_i{}^T \boldsymbol{\theta}_j; \mathbf{y}_{ij}) - \ell'(\mathbf{z}_i{}^T \boldsymbol{\theta}_j; \mathbf{y}_{ij})) \right. \right. \\
&\quad \left. \left. + (\mathbf{z}'_i - \mathbf{z}_i) \ell'(\mathbf{z}_i{}^T \boldsymbol{\theta}_j; \mathbf{y}_{ij}) \right) \right\|_2 \\
&\leq \sum_{i=1}^{n_1} [c_2 c_\theta \|\mathbf{z}'_i - \mathbf{z}_i\|_2 + c_1 \|\mathbf{z}'_i - \mathbf{z}_i\|_2] \\
&\leq (c_1 + c_2 c_\theta) \Psi(\mathbf{Z}).
\end{aligned}$$

As  $\mathbf{b}_j$  and  $\mathbf{b}'_j$  are sampled with probability proportional to

$\|\mathbf{b}\|_2^{d-1} \exp(-\beta\|\mathbf{b}\|_2)$ , we have

$$\begin{aligned} \frac{\mu(\mathbf{b}_j|G)}{\mu(\mathbf{b}'_j|G')} &= \frac{\mu(\|\mathbf{b}_j\|_2|G)/\text{surf}(\|\mathbf{b}_j\|_2)}{\mu(\|\mathbf{b}'_j\|_2|G')/\text{surf}(\|\mathbf{b}'_j\|_2)} \\ &= \frac{\|\mathbf{b}_j\|_2^{d-1} e^{-\beta\|\mathbf{b}_j\|_2}/\text{surf}(\|\mathbf{b}_j\|_2)}{\|\mathbf{b}'_j\|_2^{d-1} e^{-\beta\|\mathbf{b}'_j\|_2}/\text{surf}(\|\mathbf{b}'_j\|_2)} \\ &= \exp\left(\beta(\|\mathbf{b}'_j\|_2 - \|\mathbf{b}_j\|_2)\right) \\ &\leq \exp\left(\beta\|\mathbf{b}'_j - \mathbf{b}_j\|_2\right) \\ &\leq \exp\left(\beta(c_1 + c_2 c_\theta)\Psi(Z)\right) \end{aligned}$$

where  $\text{surf}(r)$  denotes the surface area of the sphere in  $d$  dimensions with radius  $r$ .

## B SUPPLEMENTARY THEORETICAL ARGUMENTS

### B.1 $(\epsilon, \delta)$ -Probabilistic differential privacy

*Definition B.1* ( $(\epsilon, \delta)$ -Probabilistic Differential Privacy (pDP) [51]). A randomized algorithm  $\mathcal{A}$  on domain  $\mathcal{D}$  satisfies  $(\epsilon, \delta)$ -pDP if given any neighboring datasets  $D, D' \subseteq \mathcal{D}$ , we have

$$\mathbb{P}_{o \sim \mathcal{A}(D)} \left[ e^{-\epsilon} \leq \frac{g(\mathcal{A}(D) = o)}{g(\mathcal{A}(D') = o)} \leq e^\epsilon \right] \geq 1 - \delta,$$

where  $o \sim \mathcal{A}(D)$  denotes that  $o$  follows the probabilistic distribution of the output  $\mathcal{A}(D)$ , and  $g$  denotes the probability density function.

LEMMA B.2 (LEMMA 3 IN [51]).  $(\epsilon, \delta)$ -pDP implies  $(\epsilon, \delta)$ -DP.

### B.2 Singular values of sum of matrices

*THEOREM B.3* (COROLLARY 3.4.3 IN [23]). For any  $\mathbf{A}, \mathbf{B} \in \mathbb{R}^{m \times n}$ , let  $\sigma_1(\mathbf{A}) \geq \dots \geq \sigma_q(\mathbf{A})$  and  $\sigma_1(\mathbf{B}) \geq \dots \geq \sigma_q(\mathbf{B})$  be their respective ordered singular values, where  $q = \min(m, n)$ . Let  $\sigma_1(\mathbf{A} + \mathbf{B}) \geq \dots \geq \sigma_q(\mathbf{A} + \mathbf{B})$  be the ordered singular values of  $\mathbf{A} + \mathbf{B}$ . Then

$$\sum_{i=1}^l \sigma_i(\mathbf{A} + \mathbf{B}) \leq \sum_{i=1}^l \sigma_i(\mathbf{A}) + \sum_{i=1}^l \sigma_i(\mathbf{B}), \quad l = 1, \dots, q$$

### B.3 Singular values of product of matrices

*LEMMA B.4.* For the matrices  $\mathbf{M}_1, \mathbf{M}_2$ , and  $\mathbf{M}_1 \mathbf{M}_2$ , their singular values satisfy

$$\sigma_i(\mathbf{M}_1 \mathbf{M}_2) \leq \sigma_1(\mathbf{M}_1) \sigma_i(\mathbf{M}_2)$$

where  $\sigma_i(\cdot), \forall i \in [1, N]$  denotes the eigenvalues of matrix  $\cdot$  ordered in a non-increasing order.

**Proof:** Using the min-max theorem of singular values [10] of  $\mathbf{M}_1 \mathbf{M}_2$ , we have

$$\begin{aligned} \sigma_i(\mathbf{M}_1 \mathbf{M}_2) &= \max_{S: \dim(S)=i} \min_{\mathbf{x} \in S, \|\mathbf{x}\|=1} \|\mathbf{M}_1 \mathbf{M}_2 \mathbf{x}\| \\ &\leq \max_{S: \dim(S)=i} \min_{\mathbf{x} \in S, \|\mathbf{x}\|=1} \|\mathbf{M}_1\| \cdot \|\mathbf{M}_2 \mathbf{x}\| \\ &= \sigma_1(\mathbf{M}_1) \cdot \max_{S: \dim(S)=i} \min_{\mathbf{x} \in S, \|\mathbf{x}\|=1} \|\mathbf{M}_2 \mathbf{x}\| \\ &= \sigma_1(\mathbf{M}_1) \sigma_i(\mathbf{M}_2). \end{aligned}$$

## C ADDITIONAL EXPERIMENT SETTINGS

In this section, we present additional experiment settings and results.

### C.1 Datasets.

The primary information of the used datasets is presented in Table 1, where Homo. ratio denotes the homophily ratio.

**Table 1:** Statistics of the datasets

Dataset	Vertices	Edges	Features	Classes	Homo. ratio
Cora-ML	2995	8158	2,879	7	0.81
CiteSeer	3,327	4552	3,703	6	0.71
PubMed	19,717	44,324	500	3	0.79
Actor	7600	26,659	932	5	0.22

*Definition C.1* (Homophily ratio). Given a graph  $G$  comprising vertices  $V$ , edges  $E$ , and labels  $Y$ , its homophily ratio is the proportion of edges connecting vertices with the same label. Formally,

$$\text{Homo. ratio} = \frac{1}{|V|} \sum_{v \in V} \frac{1}{|\mathcal{N}_v|} \sum_{u \in \mathcal{N}_v} \mathbb{1}(Y_u = Y_v),$$

where  $\mathcal{N}_v$  is the set of neighbors of  $v$ ,  $\mathbb{1}$  is the indicator function, and  $Y_u$  and  $Y_v$  denote the labels of vertices  $u$  and  $v$ , respectively.

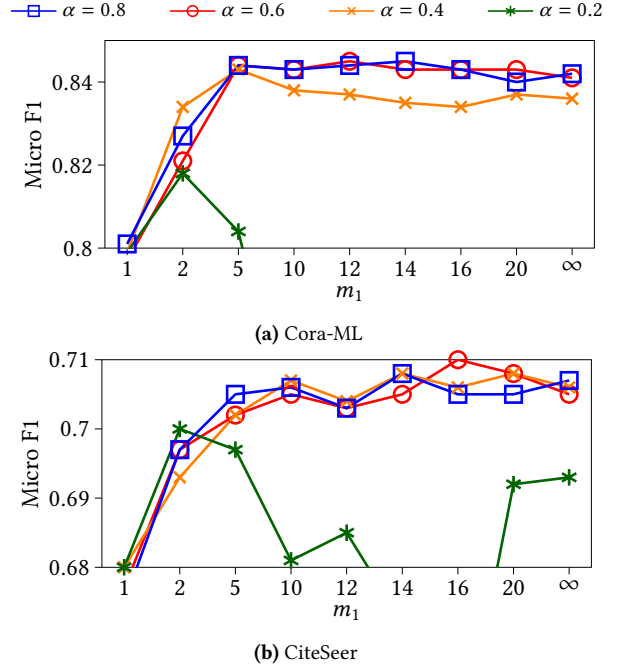


**Figure 4:** Effect of the propagation step in GCON with non-private inference under  $\epsilon = 4$ , while  $\alpha \in \{0.4, 0.5\}$ .

## C.2 Additional results of $m$

The results of GCON (NPI) under  $\epsilon = 4$  are shown in Figure 4, where  $\alpha$  is tuned in a narrow range  $\{0.4, 0.5\}$ . It uses an  $m_1$ -step propagation matrix instead of 1-step  $\hat{R}_{m_1}$  in Eq. (18). GCON (NPI) demonstrates the highest possible scores that GCON can achieve, e.g., when testing on a public and similar graph. Observe that GCON (NPI) continues to increase and tends to stabilize when  $m_1 \geq 10$ . This growth is attributed to the larger  $m_1$ , which absorbs richer information from a larger neighborhood, enabling the model to better understand the feature distribution of the vertices. Its tendency to stabilize also demonstrates that  $R_{m_1}$  with  $m_1 = 10$  is comparable in effect to  $m_1 = \infty$ .

## D FEATURE ENCODER ALGORITHM

Algorithm 4 shows the workflow of our feature encoder.

---

### Algorithm 4: FeatureEncoder( $X, Y, d$ )

---

**Input:** labeled and unlabeled features  $X = \{X_l, X_{ul}\}$ ,  
 $Y = \{Y_l, Y_{ul}\}$ , expected dimension  $d$ , a loss function  $L_{mlp}$   
**Output:** Encoded features and labels  
 $X = \{X_l, \tilde{X}_{ul}\}, Y = \{Y_l, \tilde{Y}_{ul}\}$

- 1 Initialize a MLP model  $\mathcal{M}$  with parameters  $W_1$ , a classification layer  $W_2$ , and activation functions  $H_{mlp}, H$ ;
- 2  $\tilde{X}_l = H_{mlp}(\mathcal{M}(X_l))$ ;
- 3  $\tilde{Y}_l = H(\tilde{X}_l W_2)$ ;
- 4  $W_1^*, W_2^* = \operatorname{argmin}_{W_1, W_2} L_{mlp}(\tilde{Y}_l, Y_l)$ ;
- 5  $\tilde{X} = H_{mlp}(\operatorname{MLP}(X; W_1^*))$ ;
- 6  $\tilde{Y}_{ul} = H(\tilde{X}_{ul} W_2^*)$ ;
- 7 **return**  $X = \{X_l, \tilde{X}_{ul}\}, Y = \{Y_l, \tilde{Y}_{ul}\}$ ;

---